

# Statistical relations between the parameters of aftershocks in time, space, and magnitude

Zhenqi Guo and Yoshihiko Ogata<sup>1</sup>

Department of Statistical Science, Graduate University for Advanced Studies, Tokyo

**Abstract.** The correlation between statistical parameters of seismicity, such as the  $b$  value of the *Gutenberg and Richter* [1954] relation, the  $p$  value of the modified Omori formula [*Utsu*, 1961], the  $p$  and  $\alpha$  value of the Epidemic Type Aftershock Sequence (ETAS) model [*Ogata*, 1992], and the fractal dimension  $D$  of the hypocenter distribution, is analyzed for 34 aftershock sequences in Japan from 1971 to 1995. All the parameters are estimated using maximum likelihood methods along with their error assessments. For the majority of the aftershock sequences, the ETAS model fits statistically better than the modified Omori formula, which suggests existence of clusters within the aftershock sequence. Most of the scatterplots between the estimates of the seismicity parameters in time, space, and magnitude distributions are clearly seen to be either positively or negatively correlated. The contrasting correlation patterns are revealed between the estimated parameters for the intraplate and interplate earthquakes, except for the two pairs ( $b, D$ ) and ( $\alpha, p$ ) in which similar correlation patterns are found. We focus our attention on these patterns as a source of interesting contrasts between the two earthquake groups. In particular, the significant dependence of these parameters on the depth appears to be a key to understanding the correlation pattern for interplate aftershocks, while a different interpretation is made for intraplate aftershocks because no significant dependence on depth is observed.

## Introduction

A number of statistical models have been proposed to describe seismicity characters in time, space, and magnitude. It is well known that the magnitude distribution of earthquakes in most cases satisfies the *Gutenberg and Richter* [1954] relation  $\log_{10} N = a - bM$ , where  $N$  is the total number of earthquakes with magnitude greater than  $M$  (hereinafter referred to as the Gutenberg-Richter relation). The estimated coefficient  $b$  varies mostly from 0.7 to 1.3, depending on the region. The variability of  $b$  values in different regions may be related to structural heterogeneity and stress distributions in space [*Mogi*, 1962a; *Scholz*, 1968].

It is also known that the occurrence rate of aftershock sequences in time is empirically well described by the modified Omori formula  $n(t) = K/(t+c)^p$  [*Utsu*, 1961], where  $n(t)$  is the frequency of aftershocks per unit time at time  $t$  after the main shock ( $t = 0$ ). The characteristic parameter  $p$  usually varies in value from 0.9 to 1.8, regardless of the cutoff magnitude. The variability of the  $p$  value is also related to the structural heterogeneity, stress, and temperature in the crust in some studies [*Mogi*, 1962a; *Kisslinger and Jones*, 1991]. The

parameters in the modified Omori formula can be estimated accurately by the maximum likelihood method, assuming that seismicity follows a nonstationary Poisson process [*Ogata*, 1983]. Recently, extending the modified Omori formula, *Ogata* [1988, 1989, 1992] proposed the Epidemic Type Aftershock Sequence (ETAS) model, which is a point process in which every event can produce its offspring events, more or less. The ETAS model seems to best represent the main features of regional seismicity [*Utsu et al.*, 1995].

The spatial distribution of hypocenters shows highly clustered patterns that may be related to heterogeneity of the seismic faults. Indeed, some studies showed that epicenters have a self-similar distribution in space [*Kagan and Knopoff*, 1980; *Sadovskiy et al.*, 1984]. The fractal dimension of the hypocenter distribution may be related to the heterogeneity of the fractured material. The variability of the fractal dimension in different regions may be related to geological heterogeneity [*Aviles and Scholz*, 1987].

Since the statistical parameters listed above reflect the nonhomogeneity of the seismicity distribution, relations between them are expected. For instance, *Utsu* [1961] derived the relation  $p = 4b/3$  based on a model of residual strain energy in the aftershock volume. Also, the  $b$  value is thought to be related to the fractal dimension of the fault distribution [*Aki*, 1981; *King*, 1983; *Turcotte*, 1986] based on empirical relations in which the seismic faults have a power-law dependence on size.

<sup>1</sup> Also at Institute of Statistical Mathematics, Tokyo.

Specifically, the  $b$  value is proportional to the fractal dimension  $D$ , such that  $D = 2b$ .

In order to explain the possible relations between these parameters  $b$  and  $p$  and the fractal dimension  $D$ , several theoretical models have been proposed [e.g., *Mikumo and Miyatake*, 1979; *Hirata*, 1986; *Bak and Tang*, 1989; *Ito and Matsuzaki*, 1990; *Main*, 1992; *Henderson et al.*, 1992]. For instance, *Ito and Matsuzaki* [1990] and *Matsuzaki and Takayasu* [1991] used the cellular automaton model and the stick-slip model, respectively, to simulate simultaneously the Gutenberg-Richter relation, the original Omori formula [*Omori*, 1894], and inverse power rate increase of correlation integral with respect to the distance between epicenters; but these models have no adjusting parameters to provide any different set of  $b$ ,  $p$ , and  $D$  values. *Mikumo and Miyatake* [1979] used a frictional fault model under a more realistic environment to simulate the Gutenberg-Richter relation and the modified Omori formula at the same time. From the experiments by adjusting the frictional environment, apparent negative correlation between  $p$  and  $b$  was obtained. We will see in the Discussion section that this model is quite important to understanding the results presented herein.

The analysis of the correlations between these statistical parameters based on observed earthquake data, on the other hand, is useful for providing a basis for combining the empirical relations and developing useful statistical models for seismicity. However, this aspect has not been fully examined. *Utsu* [1961] showed that there was a weak positive correlation between  $b$  and  $p$  values based on 34 aftershock data sets for demonstrating his relation. *Kisslinger and Jones* [1991] describe that such a correlation could not be found in the entire data set of aftershocks in California but, at the same time, that weak increasing trends for  $p$  against  $b$  (i.e., a positive correlation) are indicated for each separated data set of events with the strike-slip and thrust mechanisms, respectively. On the other hand, *Hirata* [1989] and *Henderson et al.* [1992] suggested a negative cross correlation between the time series of  $b$  and  $D$  values based on their data sets in Japan and California, respectively. *Guo and Ogata* [1995] estimated the parameters  $b$ ,  $p$ , and  $D$  from recent aftershock data sets in Japan to investigate correlations between the three parameters. Clear, positive correlations between any pair of these were seen for intraplate events, but this was not clear for interplate events, except for  $(b, D)$  correlation.

In this paper, we investigate such statistical parameters of aftershocks in time, space, and magnitude frequency, paying particular attention to the different features between the events within each plate and at plate boundaries. Several papers suggest discriminating features between intraplate and interplate earthquakes [e.g., *Kanamori and Anderson*, 1975; *Scholz et al.*, 1986; *Yamanaka and Shimazaki*, 1990]. Notably, interplate earthquakes have the average stress drop of about 3 MPa, while intraplate earthquake have systematically larger stress drops, about 10 MPa. This difference may be a result of the longer recurrence interval of intraplate events, possibly allowing the faults to "heal" through

chemical processes. The statistical parameters of the aftershock events that we are looking at should have some reflection of such dynamical processes and geometry of fault surfaces, so that we should also interpret our results focusing on such differences.

For such purposes, besides the reexamination of the data set used by *Guo and Ogata* [1995], we will estimate the  $p$  values using the ETAS model [*Ogata*, 1988, 1992]. The ETAS model has only five parameters, modeling clusters in temporal seismicity. Since each aftershock usually triggers its clusters, more or less,  $p$  is sometimes underestimated if we fit the modified Omori function. Thus we investigate correlations between  $p$  and the other important parameters of the ETAS,  $b$  and  $D$ , with careful consideration of the artificial correlation between the errors of the parameters. Further, we use the maximum likelihood estimation of fractal dimension along with error assessment [*Ogata and Katsura*, 1991], instead of the least squares method via the correlation integral function used by *Guo and Ogata* [1995].

## Data

The microearthquake catalog [*Matsu'ura et al.*, 1988a, b] of the Earthquake Research Institute (ERI), University of Tokyo, from June 1971 through September 1980 and the *Seismological Bulletin* of the Japan Meteorological Agency (JMA) from 1983 through 1995 are used to extract 34 data sets of aftershock sequences which took place in Japan and its vicinity. Figure 1 shows the epicenters of the corresponding main shocks.

The locations and dates of the main shocks and other details of the data are listed in Table 1. The focal depth, for instance, is given to the nearest 0.01 km in the ERI catalog for all its time span and covered area and to the nearest 0.1 km in the JMA catalog from 1983 through 1995, but in 1983, focal depths in the JMA catalog are estimated only to the nearest 1 km. The standard errors of the hypocenters provided in each catalog are mostly such that the depth is accurate to within a few kilometers and the epicenter coordinates to within 1 km, depending on the location of the hypocenter relative to the stations.

Both earthquakes occurring within the continental and the oceanic plate are classified as intraplate events. Usually, it is straightforward to identify shallow earthquakes being intraplate events, in the area where the plates do not overlap one another. In the overlapping area, careful classification is necessary. In the region of Japan and its vicinity, all interplate earthquakes take place with dip-slip-type mechanism in thrust zones, which are frictional interfaces between the subducting plate and the overriding plate, usually located in 10–60 km depth [cf. *Yoshii*, 1975]. Hypocenters of the present data are accurate enough for a shock occurring on such boundary zones to be identified. Also, the main shocks with normal or strike-slip mechanism around the thrust zones are identified as intraplate earthquakes. Those are events 17 (normal slip [cf. *Yamanaka and Shimazaki*, 1990]) and 19 (strike-slip [*Okada*, 1988]), which took place within the subducting Pacific and Philippine

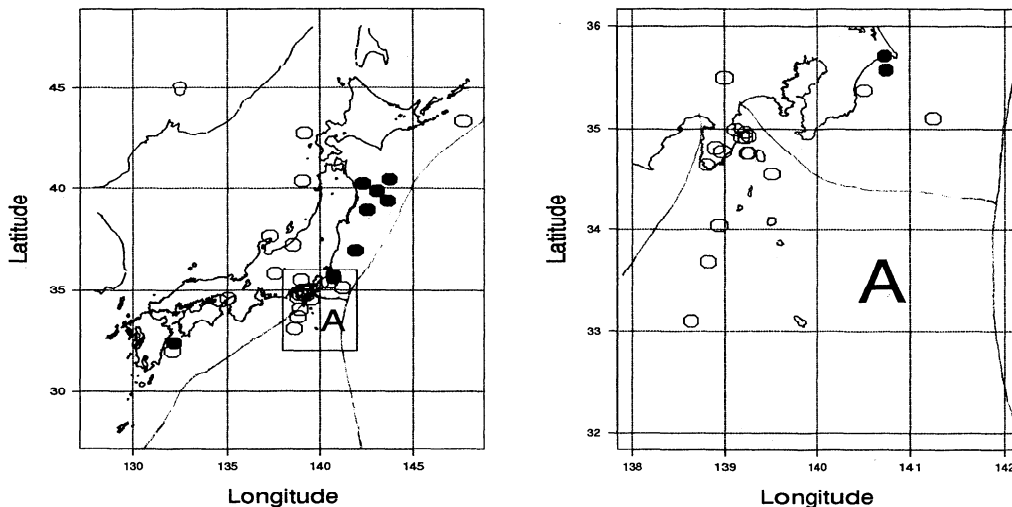


**Figure 1.** (left) The epicenters of the main shocks in the sequences analyzed. Open and solid circles indicating intraplate and interplate earthquakes, respectively. (right) Region A, including southern Kanto, the Izu peninsula, and Izu islands, magnified.

Sea Plates, respectively. Event 8 took place within the North American Plate because this is very shallow (7.5 km depth), but the epicenter is very near to event 19 (57.9 km depth). *Kikuchi and Kanamori* [1995] concluded that event 31 is an intraplate rupture within the subducting Pacific Plate based on the mechanism, depth, and high stress drop.

In spite of the suggestion that the boundary between the North American and Eurasian plates extends along the eastern margin of the Japan Sea, events 12, 25, 29, and 30 are treated as intraplate earthquakes according to the plate convergence of a small slip rate around 10 mm/yr, following *Yamanaka and Shimazaki* [1990]. Other earthquakes in inland Japan and off the south and east coast of Izu Peninsula (see region A in Figure 1) are shallow, with less than about 15 km depth. These are all identified as intraplate earthquakes.

Out of the total 34 aftershock sequences, there are 9 sequences whose main shocks took place at plate boundaries, the other 25 cases are intraplate events. There is a difficulty in obtaining more aftershock sequences of interplate events for our present analyses because the JMA's depth accuracy was poor before 1983, especially for the events in oceanic areas.

## Aftershock Distribution in Magnitude

*Utsu* [1961, 1969] showed that the *Gutenberg and Richter* [1954] relationship

$$\log_{10} N = a - bM \quad (1)$$

holds for aftershock sequence (the main shock is excluded). An estimate  $\hat{b}$  of the  $b$  value in the Gutenberg-Richter relation can be obtained by maximum likelihood [*Utsu*, 1965], which yields

$$\hat{b} = \frac{N \log_{10} e}{\sum_{i=1}^N (M_i - M_c + 0.05)}, \quad (2)$$

where  $N$  is the total number of earthquakes,  $M_c$  is the cutoff magnitude, and 0.05 is the correction constant to compensate for bias in the magnitude estimates which are rounded off to the nearest 0.1. The cutoff magnitude  $M_c$  for a sequence is the lowest magnitude above which the data set is considered complete. It may be taken as the lower bound of the interval where the cumulative log frequency curve of the magnitudes follows the linear form predicted by the Gutenberg-Richter relation. In estimating the  $b$  value of an aftershock sequence, the main shock is excluded.

The approximate standard error of the  $b$  value estimate is  $\hat{\sigma} = \hat{b}/\sqrt{N}$  [*Aki*, 1965]. The estimated  $b$  value is independent of the cutoff magnitude for a suitable range. For example, Table 2 lists estimated  $b$  values with their standard errors for events 7 and 28. The data for events 7 and 28 are taken from the ERI and JMA catalog, respectively. The estimated  $b$  value for event 7 is stable at 0.9 for cutoff magnitudes  $M_c$  ranging from 2.5 to 2.9, and the  $b$  value for event 28 is nearly equal to 1.0 for  $M_c$  ranging from 2.5 to 3.3. The estimated  $b$  values with their standard errors for the 34 data sets are listed in Table 3, where the  $\hat{b}$  values range from 0.7 to 1.4.

## Aftershock Distribution in Time Poisson Processes

The intensity function  $\lambda(t)$  of a nonstationary Poisson process is defined by

$$\lambda(t) = \lim_{\Delta \rightarrow 0} \frac{P_\Delta(t)}{\Delta}, \quad (3)$$

where  $P_\Delta(t)$  is the probability that an event occurs in a small time interval between  $t$  and  $t + \Delta$  and aftershocks are assumed independently distributed to each other. The simplest intensity model that characterizes aftershock activity is the modified Omori formula [*Utsu*, 1961], which is given by

**Table 1.** Aftershock Sequences Analyzed

Event	Date	Location		Type	Depth (km)	$M_0$	$M_c$	$T$ (days)	$N$	$M_1$	$T_1$ (days)	$\epsilon$ (km)	$R$ (km)
		Latitude	Longitude										
1	Oct. 1, 1973	35°42.2'	140°47.5'	E	49.93	5.3	2.4	60	125	4.5	20.23	1.7	5.0
2	Mar. 3, 1974	35°34.3'	140°44.8'	E	49.46	5.6	2.5	50	69	3.7	0.03	2.0	5.0
3	May. 9, 1974	34°38.5'	138°49.3'	A	2.22	6.6	2.7	200	188	4.4	0.04	0.9	3.2
4	Jul. 9, 1974	34°48.6'	138°54.5'	A	1.62	5.0	1.8	100	78	3.4	0.02	0.7	1.5
5	Jun. 16, 1976	35°29.8'	139°00.0'	A	14.06	5.9	1.8	100	108	4.0	0.06	1.0	2.3
6	Aug. 18, 1976	34°46.6'	138°58.7'	A	1.57	5.8	1.5	100	186	4.4	8.48	0.8	2.3
7	Jan. 14, 1978	34°45.7'	139°15.3'	A	3.80	7.0	2.5	200	210	5.6	0.80	0.8	3.5
8	Apr. 7, 1978	35°06.0'	141°14.2'	A	7.51	5.7	2.1	100	82	4.3	0.02	1.8	12.0
9	Dec. 3, 1978	34°55.1'	139°10.5'	A	6.67	5.8	1.8	100	175	3.4	3.76	0.3	1.8
10	Jun. 29, 1980	34°54.7'	139°13.0'	A	11.03	6.6	2.7	80	217	4.8	0.42	0.4	0.9
11	Sep. 10, 1980	34°02.5'	138°56.8'	A	3.20	4.7	2.2	20	90	4.5	0.01	0.9	3.5
12	May. 26, 1983	40°21.4'	139°04.6'	A	14.	7.7	3.8	200	530	7.1	26.14	1.7	23.0
13	Aug. 7, 1984	32°22.8'	132°09.3'	E	33.	7.1	2.9	100	145	4.8	3.30	1.5	5.5
14	Sep. 14, 1984	35°49.3'	137°33.6'	A	2.	6.8	3.5	100	72	6.2	0.94	1.3	3.0
15	Nov. 22, 1986	34°32.8'	139°31.5'	A	15.1	6.0	2.9	100	265	4.5	54.73	1.3	4.0
16	Feb. 6, 1987	36°56.2'	141°56.1'	E	35.0	6.7	3.3	60	78	5.6	21.73	5.0	12.0
17	Mar. 18, 1987	31°58.2'	132°03.8'	A	48.1	6.6	2.6	100	98	5.1	5.06	1.0	4.0
18	May. 11, 1987	34°55.7'	139°15.5'	A	14.9	5.0	2.9	30	98	4.9	0.39	0.5	1.4
19	Dec. 17, 1987	35°22.3'	140°29.8'	A	57.9	6.7	2.8	100	232	5.2	30.40	1.0	5.0
20	Jul. 31, 1988	34°57.8'	139°13.0'	A	5.1	5.2	2.9	40	336	5.2	2.45	0.4	1.9
21	Jul. 9, 1989	34°59.5'	139°06.7'	A	3.4	5.5	2.0	100	245	4.8	5.18	0.3	1.0
22	Nov. 2, 1989	39°51.3'	143°03.4'	E	0.0	7.1	3.3	100	354	6.3	0.01	5.0	17.0
23	Feb. 20, 1990	34°45.6'	139°14.0'	A	5.8	6.5	2.2	10	152	5.1	0.02	1.0	4.0
24	Sep. 24, 1990	33°06.2'	138°38.0'	A	60.0	6.6	2.9	100	76	6.0	0.04	1.8	4.0
25	Dec. 7, 1990	37°12.4'	138°33.6'	A	14.9	5.4	2.6	100	123	5.3	0.01	1.1	3.0
26	Sep. 3, 1991	33°41.0'	138°49.9'	A	33.1	6.3	2.9	100	146	4.8	0.45	2.0	5.0
27	Jul. 18, 1992	39°22.8'	143°39.3'	E	0.0	6.9	3.0	200	497	6.4	0.07	4.0	20.0
28	Dec. 28, 1992	38°55.5'	142°33.0'	E	33.5	5.9	2.5	200	704	5.8	3.63	0.5	6.0
29	Feb. 7, 1993	37°39.2'	137°18.0'	A	24.8	6.6	2.9	100	182	5.0	8.14	2.0	5.0
30	Jul. 2, 1993	42°46.8'	139°11.0'	A	35.1	7.8	3.4	150	1517	6.3	26.17	1.0	9.0
31	Oct. 4, 1994	43°22.3'	147°42.5'	A	23.0	8.1	4.0	200	944	7.0	4.77	3.0	10.0
32	Dec. 28, 1994	40°25.6'	143°44.9'	E	0.0	7.5	3.0	200	796	6.5	0.43	3.0	9.0
33	Jan. 7, 1995	40°13.2'	142°18.5'	E	47.8	7.2	3.0	200	325	6.2	0.17	1.2	3.0
34	Jan. 17, 1995	34°35.6'	135°02.1'	A	17.9	7.2	2.5	200	825	5.4	0.08	0.2	1.0

Events 1-11 are obtained from the catalog by the Earthquake Research Institute (ERI), University of Tokyo, and events 12-34 are from the Japan Meteorological Agency (JMA) catalog. "A" indicates intraplate earthquakes; "E" indicates interplate earthquakes.  $M_0$  is the magnitude of the main shock,  $M_c$  is the cutoff magnitude,  $T$  is span of observed time interval.  $N$  is the number of aftershocks whose magnitude is equal to or greater than  $M_c$ . The modified Omori formula [Utsu, 1961] and Epidemic Type Aftershock Sequence (ETAS) models [Ogata, 1992] are estimated by the events in the time interval  $(0, T)$ .  $M_1$  is the magnitude of the biggest aftershock in sequence.  $T_1$  is the time interval from the main shock to the biggest aftershock occurred. Fractal dimension is estimated from the distance range  $[\epsilon, R]$ .

$$\lambda_\theta(t) = \frac{K}{(t+c)^p}, \quad \theta = (K, c, p), \quad (4)$$

where  $t$  is the lapse time after the main shock and  $\theta = (K, c, p)$  are parameters to be estimated. Ogata [1983] suggested estimating  $\theta$  from the record of occurrence times  $\{t_i; i = 1, 2, \dots, N\}$  by maximum likelihood.

It is often the case that the aftershock sequence contains secondary aftershocks. Utsu [1970] showed that such complex sequences can be represented by the superposition of some modified Omori functions

$$\lambda_\theta(t) = \sum_{m=1}^M \frac{K_m}{(t-\tau_m+c_m)^{p_m}}, \quad \theta = (K_m, c_m, p_m), \quad m = 1, 2, \dots, M, \quad (5)$$

which depend on the history of origin times  $\tau_m$  ( $0 = \tau_1 < \tau_2, \dots, \tau_m$ ) of triggering events of the secondary aftershocks, and the sum  $\sum_{\tau_m < t}$  is taken for all triggering events  $m = 1, 2, \dots, M$  that satisfy  $\tau_m < t$ . Statistical analyses of complex aftershock sequences showed that the model (5) often fits the data well for suitable  $\tau_m$  and  $M$  [Ogata, 1983; Ogata and Shimazaki, 1984].

### ETAS Model

It is generally not easy to obtain a complete aftershock data set from a catalog, especially in an area of high seismic activity, such as plate boundary zones, because the selected data set may contain background events. Also, it is sometimes difficult to identify trigger-

**Table 2.** Parameters of Events 7 and 28 for Various Cutoff Magnitudes  $M_c$ 

$M_c$	$N$	$\hat{b}$	$\hat{D}$	$\hat{K}_0$	$\hat{c}$	$\hat{\alpha}$	$\hat{p}_e$
<i>Event 7, Intraplate</i>							
2.5	210	0.922 (0.064)	2.179 (0.081)	0.013 (0.006)	0.037 (0.016)	1.587 (0.157)	1.160 (0.050)
2.6	170	0.924 (0.071)	2.173 (0.101)	0.013 (0.007)	0.033 (0.016)	1.560 (0.174)	1.182 (0.056)
2.7	141	0.952 (0.080)	2.270 (0.123)	0.010 (0.007)	0.031 (0.015)	1.632 (0.206)	1.190 (0.059)
2.8	105	0.876 (0.085)	2.270 (0.182)	0.007 (0.006)	0.031 (0.017)	1.692 (0.232)	1.185 (0.065)
2.9	88	0.901 (0.096)	2.105 (0.186)	0.008 (0.006)	0.024 (0.015)	1.658 (0.239)	1.154 (0.067)
<i>Event 28, Interplate</i>							
2.5	704	0.924 (0.035)	2.431 (0.015)	0.75E-4 (0.15E-3)	0.108 (0.031)	3.856 (0.629)	1.012 (0.029)
2.6	585	0.954 (0.039)	2.444 (0.013)	0.32E-4 (0.75E-4)	0.097 (0.031)	4.186 (0.744)	1.014 (0.031)
2.7	485	0.989 (0.045)	2.431 (0.015)	0.27E-4 (0.29E-4)	0.079 (0.028)	4.300 (0.349)	0.996 (0.033)
2.8	392	1.007 (0.051)	2.419 (0.017)	0.66E-5 (0.98E-5)	0.067 (0.027)	4.841 (0.499)	0.996 (0.035)
2.9	312	1.012 (0.057)	2.395 (0.021)	0.13E-4 (0.43E-4)	0.069 (0.033)	4.711 (1.162)	1.017 (0.042)
3.0	254	1.045 (0.066)	2.552 (0.034)	0.40E-4 (0.16E-3)	0.097 (0.053)	4.431 (1.423)	1.058 (0.052)
3.1	200	1.048 (0.074)	2.496 (0.039)	0.85E-3 (0.19E-2)	0.047 (0.030)	3.292 (0.883)	1.032 (0.051)
3.2	153	1.018 (0.082)	2.495 (0.049)	0.76E-2 (0.12E-1)	0.028 (0.020)	2.355 (0.718)	1.055 (0.061)
3.3	119	1.001 (0.092)	2.479 (0.068)	0.86E-2 (0.96E-2)	0.019 (0.014)	2.260 (0.553)	1.028 (0.058)

Maximum likelihood parameter estimates for events 7 and 28 for the time interval  $(0, T)$  and distance range  $[\varepsilon, R]$  in Table 1.  $N$  is the total number of aftershocks with  $M \geq M_c$ ,  $\hat{b}$  is the maximum likelihood estimates (MLEs) of the coefficient in Gutenberg and Richter[1954] relation,  $\hat{D}$  is the MLEs of the fractal dimension of the hypocenter distribution, and  $\hat{K}_0$ ,  $\hat{c}$ ,  $\hat{\alpha}$ , and  $\hat{p}_e$  are the MLEs of the ETAS model. Numbers in parenthesis are standard errors.

ing events as the threshold magnitude of the data decreases. Moreover, the models in (4) and (5) do not use magnitude data. To overcome these weaknesses, Ogata [1988, 1989, 1992] introduced the Epidemic Type After-shock Sequence (ETAS) model, which extends model (5).

The ETAS model includes a parameter  $\mu$  to model the background seismicity as a stationary Poisson process. In the ETAS model, an earthquake occurring at time  $t_i$  can generate aftershocks at a rate that decreases according to the modified Omori formula

$$\nu_i(t) = \frac{K_i}{(t - t_i + c)^p}, \quad t > t_i, \quad (6)$$

where  $K_i$  is proportional to the expected number of aftershocks whose magnitudes exceed the cutoff magnitude  $M_c$ , generated by an event of magnitude  $M_i$ . The model fits well if  $K_i$  is of the form

$$K_i = K_0 e^{\alpha(M_i - M_c)}, \quad (7)$$

where  $K_0$  and  $\alpha$  are parameters to be estimated. Thus, the ETAS model is defined in terms of the intensity function (3) by the superposition

$$\lambda_\theta(t) = \mu + \sum_{t_i < t} \nu_i(t), \quad \theta = (\mu, K_0, c, \alpha, p), \quad (8)$$

which depends on the history of occurrence times and magnitudes before time  $t$ ,  $\{(t_i, M_i) : t_i < t\}$ , and the sum  $\sum_{t_i < t}$  is taken for all events  $i$  such that  $t_i < t$ . The

parameter  $\theta = (\mu, K_0, c, \alpha, p)$  is assumed to take the same values for all events, thus representing regional characteristics of seismicity. Most  $p$  and  $c$  values obtained for various earthquake data sets fall in the range [0.9, 1.4] and [0.003, 0.3 days], respectively. The parameter  $\alpha$ , which is typically between 0.2 and 3.0, measures an efficiency with which events above the threshold magnitude generate offspring and is useful in characterizing earthquake sequences quantitatively in relation to the classification into seismic types [Utsu, 1970; Ogata, 1992]. For example, earthquake swarms have  $\alpha$  values less than 1, and clear and simple mainshock-aftershock activity in Japan and its vicinity has  $\alpha > 2$ .

#### Values of $p$ and $\alpha$ of the Sequences

The spatial area and time span are carefully chosen for the 34 data sets to exclude the background seismicity, so that  $\mu$  in (8) can be disregarded (i.e.,  $\mu = 0$ ). The  $p$  and  $\alpha$  estimates for a range of different cutoff magnitudes  $M_c$  take almost the same values up to the standard error as shown in Table 2 for events 7 and 28, for example (see appendix for the estimation method).

Hereafter, the symbol  $p_o$  denotes the  $p$  value in the modified Omori formulae (4) and (5) and  $p_e$  denotes the one in the ETAS model (8). The estimates of  $p_o$ ,  $p_e$ , and  $\alpha$  for 34 aftershock sequences are listed with their standard errors in Table 3, in which the  $p_o$  value estimated for the model (5) is further discriminated from the one for the model (4); actually, we assume that there is, at most, a single sequence of secondary after-

**Table 3.** Estimated Parameters and Corresponding Akaike Information Criterion Values

Event	$\hat{b}$	$\hat{D}$	$\hat{\alpha}$	$\hat{p}_e$	$\hat{p}_o$	Type	$\Delta \text{AIC}$
1	0.945 (0.085)	2.215 (0.138)	3.956 (0.601)	0.960 (0.049)	0.926 (0.052)		-7.2
2	1.164 (0.140)	2.274 (0.248)	3.709 (0.671)	0.988 (0.104)	0.987 (0.106)		2.0
3	1.120 (0.082)	2.601 (0.130)	2.046 (0.270)	1.146 (0.049)	1.120 (0.045)		0.2
4	0.903 (0.102)	2.268 (0.304)	1.752 (0.280)	1.027 (0.082)	0.930 (0.071)		-6.4
5	0.652 (0.063)	2.344 (0.178)	1.971 (0.258)	0.966 (0.051)	0.945 (0.049)	2nd	6.4
6	0.810 (0.059)	2.394 (0.088)	1.194 (0.115)	1.106 (0.063)	0.999 (0.059)		-61.2
7	0.922 (0.064)	2.179 (0.080)	1.587 (0.158)	1.160 (0.050)	1.114 (0.042)	2nd	10.2
8	0.692 (0.076)	2.207 (0.110)	1.750 (0.256)	0.844 (0.058)	0.793 (0.063)		-20.4
9	0.958 (0.072)	2.310 (0.079)	0.886 (0.125)	1.265 (0.050)	1.278 (0.080)	2nd	-213.0
10	1.294 (0.088)	2.688 (0.202)	0.659 (0.140)	1.304 (0.047)	1.581 (0.180)		-436.2
11	1.083 (0.114)	2.834 (0.187)	1.638 (0.252)	1.277 (0.108)	1.367 (0.172)		-25.8
12	0.984 (0.043)	2.354 (0.023)	2.130 (0.174)	1.209 (0.049)	1.148 (0.035)	2nd	-8.0
13	1.033 (0.086)	2.621 (0.109)	2.878 (0.494)	1.003 (0.052)	1.002 (0.054)		2.0
14	0.914 (0.108)	2.494 (0.251)	1.927 (0.378)	1.110 (0.068)	1.078 (0.062)	2nd	6.4
15	1.342 (0.082)	2.384 (0.105)	1.165 (0.157)	1.436 (0.067)	1.927 (0.076)	2nd	24.6
16	0.878 (0.099)	2.284 (0.155)	2.154 (0.367)	1.060 (0.081)	0.905 (0.065)		-46.0
17	0.831 (0.084)	2.372 (0.195)	2.095 (0.308)	0.986 (0.051)	0.955 (0.045)	2nd	12.8
18	1.405 (0.142)	2.491 (0.232)	1.283 (0.256)	1.208 (0.066)	1.492 (0.067)	2nd	-23.2
19	0.844 (0.055)	2.411 (0.059)	1.620 (0.109)	1.051 (0.048)	0.931 (0.040)	2nd	-33.8
20	0.903 (0.049)	2.573 (0.053)	0.547 (0.268)	1.550 (0.083)	1.240 (0.140)	2nd	-142.4
21	0.834 (0.053)	2.559 (0.102)	1.203 (0.163)	1.272 (0.075)	1.403 (0.083)		-2.6
22	0.795 (0.042)	2.043 (0.102)	1.830 (0.178)	1.131 (0.055)	0.944 (0.044)		-80.4
23	0.742 (0.060)	2.029 (0.076)	2.777 (0.395)	1.043 (0.081)	1.044 (0.085)		2.0
24	0.654 (0.075)	2.353 (0.242)	3.323 (0.562)	1.234 (0.098)	1.255 (0.099)		2.0
25	0.775 (0.070)	2.308 (0.120)	2.446 (0.327)	1.012 (0.050)	0.936 (0.046)		-14.6
26	1.068 (0.088)	2.237 (0.125)	1.801 (0.205)	1.210 (0.085)	1.104 (0.067)		-5.4
27	0.752 (0.034)	2.095 (0.041)	1.494 (0.129)	1.170 (0.037)	1.124 (0.031)	2nd	-103.8
28	0.989 (0.045)	2.431 (0.015)	4.300 (0.349)	0.996 (0.033)	0.984 (0.036)	2nd	-6.0
29	0.916 (0.068)	2.197 (0.127)	2.657 (0.414)	0.899 (0.046)	0.884 (0.044)	2nd	1.6
30	1.297 (0.033)	2.490 (0.018)	1.369 (0.079)	1.425 (0.057)	1.233 (0.036)		-66.4
31	0.972 (0.032)	2.656 (0.047)	2.806 (0.300)	1.061 (0.034)	1.038 (0.030)		-4.2
32	0.781 (0.028)	2.037 (0.066)	1.228 (0.085)	1.165 (0.032)	0.883 (0.026)		-495.4
33	0.992 (0.055)	2.409 (0.220)	1.718 (0.129)	0.859 (0.039)	0.763 (0.027)		-2.8
34	0.957 (0.033)	2.691 (0.054)	1.546 (0.087)	1.175 (0.003)	1.021 (0.042)		-32.8

Here  $p_e$  and  $p_o$  are the parameters of the ETAS model and the modified Omori formula, respectively.  $\text{AIC}_e$  and  $\text{AIC}_o$  are the values of Akaike information criterion (AIC) [Akaike, 1974] of the ETAS model and the modified Omori formula, respectively. The "2nd" indicates that the data include conspicuous secondary aftershocks and the same  $p$  value is used in (5). The  $\Delta \text{AIC} = \text{AIC}_e - \text{AIC}_o$ . Negative  $\Delta \text{AIC}$  indicates the degree of significance that the ETAS model is preferred. Numbers in parenthesis are standard errors.

shocks and that  $p_1 = p_2 = p_o$ , so that five parameters  $\theta = (K_1, K_2, c_1, c_2, p_o)$  are used in (5) with  $M = 2$ . In the ETAS model the  $\hat{p}_e$  estimates vary from 0.8 to 1.4. The scatterplot of  $(\hat{p}_e, \hat{p}_o)$  in Figure 2 shows that  $\hat{p}_e$  is about equal to or larger than  $\hat{p}_o$  for the same data, except when  $\hat{p}_o$  is extraordinarily large. Such exceptions with  $p_e < p_o$  are all from the Izu area (events 10, 11, 15, 18, and 21), and these aftershock sequences include magma-related swarms within the aftershock volumes. This is one of the seismic characteristics in and around the Izu peninsula [Utsu, 1981; Matsu'ura, 1983].

From Figure 2a, most of the  $\hat{p}_o$  and  $\hat{p}_e$  values for intraplate earthquakes are larger than 1.0 with large variability in the distribution, while those for interplate earthquakes are around 1.0 with small variability. The estimates of  $\hat{\alpha}$  mostly range from 0.8 to 3.5. For example, the data sets for events 9, 10, 20, and 23, which

yield small  $\hat{\alpha}$ , are close to swarm-type sequences as a whole.

For each aftershock sequence, we compare the Akaike information criterion (AIC) [Akaike, 1974] (see appendix) of the ETAS model (8) with that of the modified Omori formula (4) or its extended case (5) with  $M = 2$ . We calculate the AIC for the ETAS model (8) with four parameters  $(K_0, c, \alpha, p_e)$ , for the modified Omori model (4) with three parameters  $(K, c, p_o)$ , and also for the extended formula (5) with five parameters  $(K_1, K_2, c_1, c_2, p_o)$ .

We use  $\text{AIC}_o$  to denote the AIC values in the modified Omori formulas (4) and (5) and  $\text{AIC}_e$  to denote the one in the ETAS model (8). The difference  $\Delta \text{AIC} = \text{AIC}_e - \text{AIC}_o$  is listed for each aftershock sequence in Table 3, in which  $\text{AIC}_e$  values are smaller than the corresponding  $\text{AIC}_o$  value (i.e.,  $\Delta \text{AIC} < 0$ ) for 25 cases

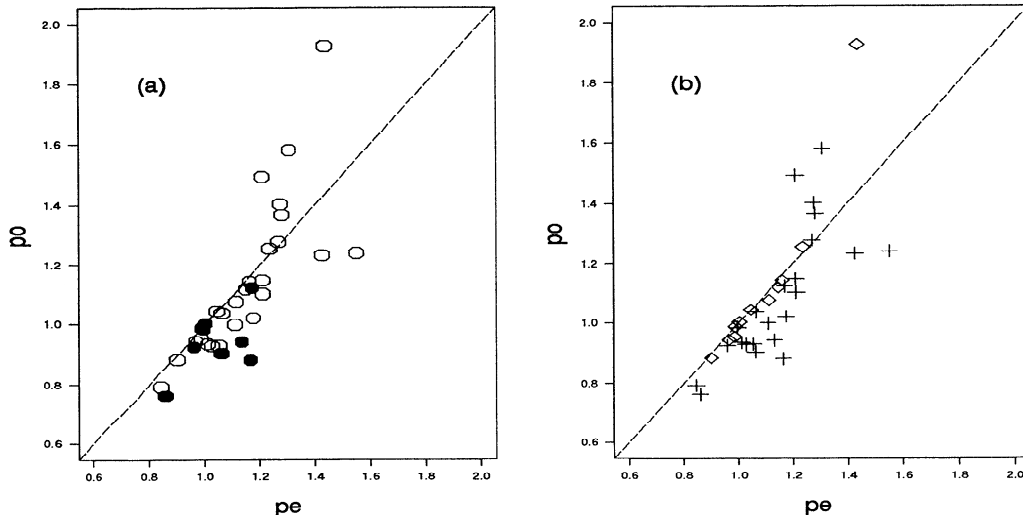


**Figure 2.** Scatterplots of  $\hat{p}_e$  versus  $\hat{p}_o$ . (a) Open and solid circles indicating intraplate and interplate earthquakes, respectively. (b) Pluses and diamonds indicating the cases where the Epidemic Type Aftershock Sequence (ETAS) [Ogata, 1992] and the modified Omori models [Utsu, 1961] are selected by the Akaike information criterion (AIC) [Akaike, 1974], respectively.

out of 34. This indicates that the ETAS model is often preferred by AIC to the modified Omori formulas; this appears to be the case because it models the time clusters within aftershock sequence. In the case where the modified Omori model has smaller AIC, the estimated  $\alpha$  of the ETAS model applied to the same data usually has a value larger than 2 (less clusters within the aftershock sequence) and also,  $\hat{p}_e$  is almost equal to  $\hat{p}_o$  (Figure 2b), except for the case of event 15. This means that the ETAS model for such data is close enough to the modified Omori formula. For the case of event 15, where the  $\hat{p}_o$  is very large, the sequence includes swarms associated with the eruption of the Izu-Oshima volcano in the aftershock volume. Also, it should be remembered that the ETAS model assumes the same values of the parameters throughout the aftershock sequence. Therefore, when the  $p$  or  $\alpha$  of conspicuous secondary aftershocks is significantly different from that of the primary ones, the good fit of the ETAS model is not expected. After all, it is shown that, in general, the ETAS model is a natural extension of the modified Omori formulas for aftershock sequences.

Figure 3 shows an example where the Poisson model for the modified Omori formula showed a poor fit to the data. The occurrence times within the aftershock sequence of event 10 are highly clustered, although the decaying trend itself obeys the modified Omori formula. In Figure 3a, we can clearly see clusters in the "residual events" in the transformed occurrence times (see appendix). On the other hand, we see that those events in Figure 3b are rather uniformly distributed (closer to the stationary Poisson process), which shows an apparent better fit of the ETAS to the data than the Poisson model.

Figure 4 shows scatterplots of  $\hat{\alpha}$  against  $\hat{p}_e$  with the joint standard errors (see appendix), from which we see little correlation between the errors of  $\hat{\alpha}$  and  $\hat{p}_e$  for

each aftershock sequence. On the other hand, in the same figure, a clear negative correlation can be seen in the scatterplot of  $\alpha$  against  $p$  value for the independent 34 data sets. The estimated correlation coefficients are  $-0.570$  for intraplate earthquakes and  $-0.506$  for interplate earthquakes. The statistical significance of the correlation can be tested using the likelihood ratio statistic and also Fisher's  $z$  test statistic, which are listed in Table 4. Furthermore, pairs  $(\hat{\alpha}, \hat{p}_e)$  for intraplate and interplate earthquakes can be discriminated; most  $\hat{\alpha}$  values are smaller than 2.0 with high  $\hat{p}_e$  values and large variability for intraplate earthquakes, while  $\hat{\alpha}$  values are large with  $\hat{p}_e$  values distributing around 1.0 for interplate events. Similar negative correlations but with significantly different slopes are seen between the two groups in Figure 4.

### Aftershock Distribution in Space

Some studies [Kagan and Knopoff, 1980; Guo and Ogata, 1995] showed that the spatial autocovariance between pairs of hypocenters obeys the inverse power law

$$c(\mathbf{r}) \sim Cr^{-H} \quad (9)$$

for a range of distance  $r = |\mathbf{r}|$ , where  $H$  is a constant called the self-similarity index or Hurst number. The fractal dimension  $D$  is related to  $H$  by  $D = 3 - H$  [Mandelbrot, 1982; Grassberger, 1983]. If we can assume the relation in (9) for a range of distance of  $\varepsilon \leq r \leq R$ , the fractal dimension of a spatial point pattern can be estimated by the maximum likelihood method, modeling the Palm intensity [Ogata and Katsumura, 1991]. Palm intensity function,  $\lambda(\mathbf{r}|\mathbf{r}')$ , is defined as the local intensity of an event taking place at  $\mathbf{r}$  given the existence of the other event at  $\mathbf{r}'$ ; thus

$$\lambda(\mathbf{r}|\mathbf{r}')d\mathbf{r} = Pr[N(d\mathbf{r}) = 1 | N(\mathbf{r}') = 1], \quad (10)$$

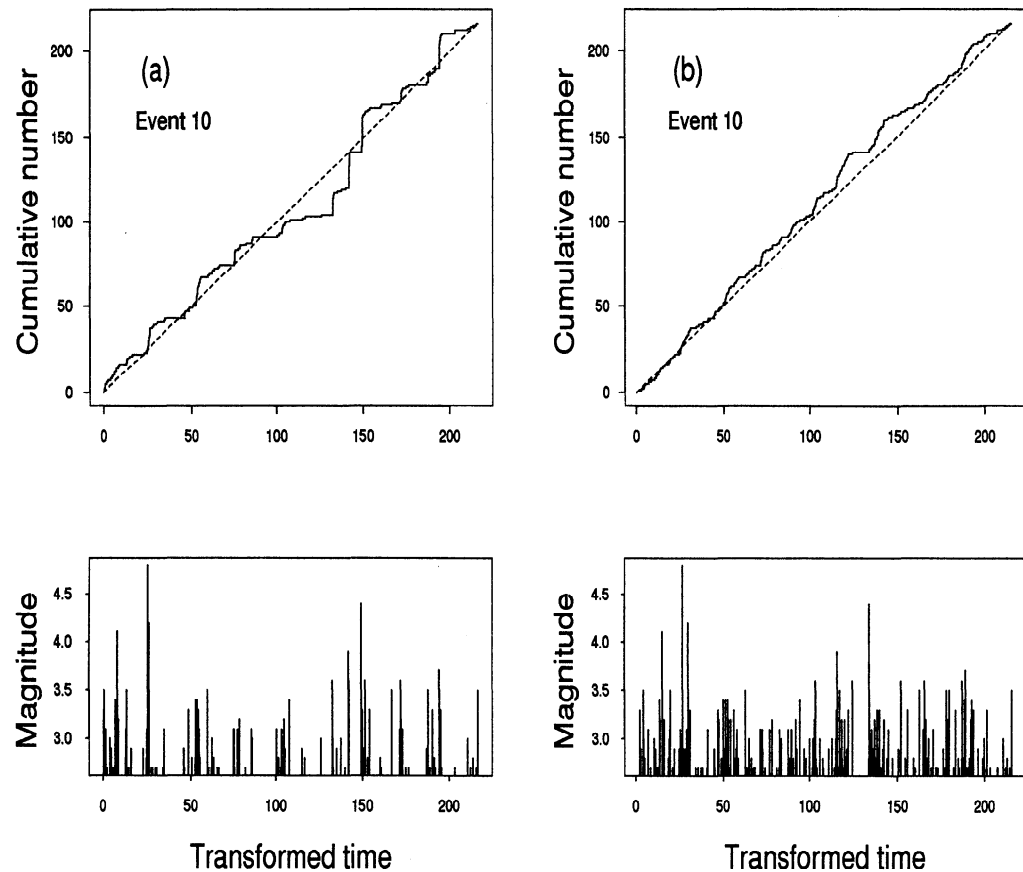


**Figure 3.** Diagrams of cumulative number and magnitude of aftershocks of event 10 versus transformed time, which is obtained by fitting (a) the modified Omori formula and (b) the ETAS model, respectively. See appendix for the method of the residual analysis for point processes.

where  $N(dr)$  is the number of events in a volume  $dr = dx dy dz$ . Assume that the Palm intensity is only dependent of the distance  $r = |\mathbf{r} - \mathbf{r}'|$  between the events. Then, we can assume  $\mathbf{r}'$  to be the coordinates'

origin without loss of generality. From relation (9), the Palm intensity in (10) can be expressed in terms of  $H$  (see appendix):

$$\lambda_\theta(\mathbf{r}) = \mu + \frac{K}{r^H}, \quad \varepsilon \leq r \leq R, \quad (11)$$

where  $\theta = (\mu, K, H)$  are parameters to be estimated. From (11), we see that smaller fractal dimension  $D = 3 - H$  means that the clusters of events are distributed tighter in the volume and vice versa. Therefore smaller  $D$  means higher heterogeneity of fractures. These parameters, along with their standard errors, are estimated by the maximum likelihood method assuming a nonstationary Poisson point process in the three dimensional volume of the range  $\varepsilon \leq r \leq R$  (see appendix).

Aftershocks with reported focal depths equal to 0.0 km were removed from the analysis of fractal dimension. For each event, we list in Table 1 the distance range  $[\varepsilon, R]$  used to estimate the fractal dimension. The distance ranges were determined by inspecting the linearity of the cumulative distribution of  $N(r)$  versus distance  $r$  of hypocenter pairs in log-log scales, where  $N(r)$  is number of pairs of hypocenters whose three-dimensional distances are smaller than  $r$ . Figure 5 is an example of a plot of  $N(r)$  versus  $r$  on a log-log scale. Usually, the upper limit of the range  $r$  is taken around a quarter to one third of the thickness of aftershock volume and the lower limit is taken around 0.3 to a few

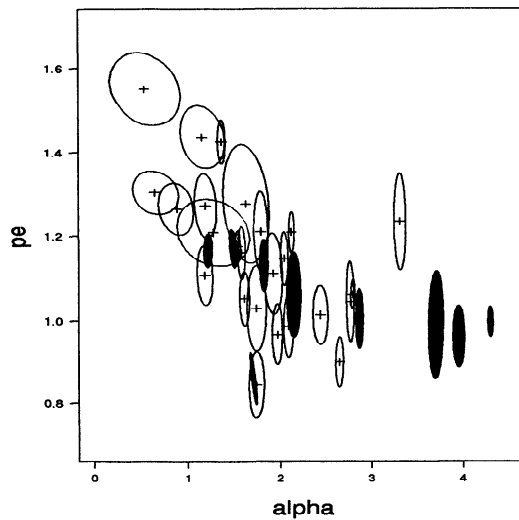


**Figure 4.** Scatterplot of the maximum likelihood estimates (MLEs) of two characteristic parameters of the ETAS model,  $\hat{p}_e$  versus  $\hat{\alpha}$ , where the ellipses indicating the joint standard error (see appendix) with open and solid ellipses indicating those of intraplate and interplate earthquakes, respectively.

**Table 4.** Correlations Between Parameters

Correlation	$\rho$	$\Lambda$	$Z_n$	Confidence	Slope
<i>Intraplate, n = 25</i>					
$\hat{\alpha}, \hat{p}_e$	-0.570	9.8	3.037	clear	-0.147
$\hat{b}, \hat{p}_e$	0.572	9.9	3.053	clear	0.697
$\hat{b}, \hat{D}$	0.427	5.0	2.142	clear	0.809
$\hat{p}_e, \hat{D}$	0.457	5.9	2.317	clear	1.294
$\hat{\alpha}, \hat{b}$	-0.472	6.3	2.404	clear	-0.155
$\hat{\alpha}, \hat{D}$	-0.347	3.2	1.698	weak	-0.104
<i>Interplate, n = 9</i>					
$\hat{\alpha}, \hat{p}_e$	-0.506	2.7	1.365	weak	-0.046
$\hat{b}, \hat{p}_e$	-0.764	7.9	2.465	clear	-0.706
$\hat{b}, \hat{D}$	0.704	6.2	2.143	clear	1.671
$\hat{p}_e, \hat{D}$	-0.695	5.9	2.102	clear	-2.382
$\hat{\alpha}, \hat{b}$	0.702	6.1	2.132	clear	0.083
$\hat{\alpha}, \hat{D}$	0.473	2.3	1.260	weak	0.082

Here  $\rho$  indicates the estimated correlation coefficient between variables in the correlation column. The  $\Lambda$  is the log likelihood ratio.  $Z_n = z\sqrt{n-3}$ , where  $z$  is Fisher's  $z$  transformation and  $n$  is the number of estimate pairs. See text for description of "clear" and "weak". Slopes are estimated by the principal component analysis (see appendix).

kilometers, which corresponds to the relative error of the locations. Table 2 illustrates the stability of the estimated fractal dimension  $D$  relative to its standard error for events 7 and 28. The estimated fractal dimensions of all aftershock sequences and their standard errors are listed in Table 3.

### Correlations Between the Parameters

In order to discuss the correlations between the characteristic parameters estimated for 34 aftershock sequences (namely,  $\alpha$  and  $p_e$  of the ETAS model,  $b$  of the Gutenberg-Richter relation, and the fractal dimension  $D$  of the hypocenter distribution), the aftershock sequences are divided into two groups, those of intraplate and interplate earthquakes. Scatterplots of every pair of variables  $(b, p_e)$ ,  $(b, D)$ ,  $(p_e, D)$ ,  $(\alpha, b)$ , and  $(\alpha, D)$  for intraplate and interplate earthquakes are shown in Figures 6-10.

The significance of the correlations  $\hat{\rho}$  between the estimated parameters is examined using both the likelihood ratio test (see appendix) and the statistic  $Z_n = \hat{z}\sqrt{n-3}$ , which varies according to the normal distribution  $N(\hat{z}, 1^2)$ , where  $\hat{z} = \ln(1-\hat{\rho})/(1+\hat{\rho})$  is Fisher's  $z$  statistic and  $n$  is the number of the pairs. If the likelihood ratio statistic satisfies  $\Lambda > 2.0$ , which corresponds with the AIC choosing the correlated model (see appendix), and also if  $|Z_n| > 1.96$  holds under the assumption of  $\rho = 0$ , the estimated correlation of the scatterplots is significantly nonzero at the 95% level. If

$\Lambda > 2.0$  but  $1.0 < |Z_n| < 1.96$ , we consider the significance of the correlation to be weak; it is nonzero at 67% significance. If  $\Lambda < 2.0$  and  $|Z_n| < 1.0$ , there is no evidence for a nonzero correlation between the pairs. Table 4 lists the correlation coefficients, log likelihood ratio values, and  $Z_n$  for the pairs  $(\alpha, p_e)$ ,  $(b, p_e)$ ,  $(b, D)$ ,  $(p_e, D)$ ,  $(\alpha, b)$ , and  $(\alpha, D)$  separately for intraplate and interplate earthquakes.

The scatterplot in Figure 6a shows a clear positive correlation between  $\hat{b}$  and  $\hat{p}_e$  for intraplate earthquakes. The points  $(\hat{b}, \hat{p}_e)$  are superimposed by Utsu's relation  $p = 4b/3$  (Figure 6a, solid line). On the other hand, Figure 6b indicates a clear negative correlation between  $\hat{b}$  and  $\hat{p}_e$  for interplate earthquakes. The estimated slope (Figure 6b, dashed line) of the scatterplot is -0.706, which is obtained from the first principal component of the scatterplot (see appendix).

The scatterplots in Figures 7a and 7b show clear positive correlations between  $\hat{b}$  and  $\hat{D}$  for both intraplate and interplate earthquakes. Those plots and their slopes are consistent with Aki's [1981] relation  $D = 2b$  (solid lines), except for those with  $\hat{b} > 1.2$ , although it lies a little below and to the right. Here it should be noted that the  $D$  in Aki's relation is the fractal dimension of the faults' configuration but that the  $D$  for the scatterplot is the dimension of the hypocenter distribution [Main, 1992]. Also, it should be noted that the difference of  $\hat{D}$  that is expected from Aki's line in Figure 7a (i.e.,  $\hat{D} - 2\hat{b}$ ) is clearly larger, on average, than that in Figure 7b. In other words, for a fixed fractal dimension  $D$  of hypocenter distribution,  $b$  values for aftershocks within a plate distribute systematically smaller than those at a plate boundary. This implication will be discussed in the next section.

Incidentally, the present positive correlation between  $\hat{b}$  and  $\hat{D}$  contradicts the negative correlation estimated by Hirata [1989] and Henderson et al. [1992]. Hirata [1989], using data from shallow earthquakes with mag-

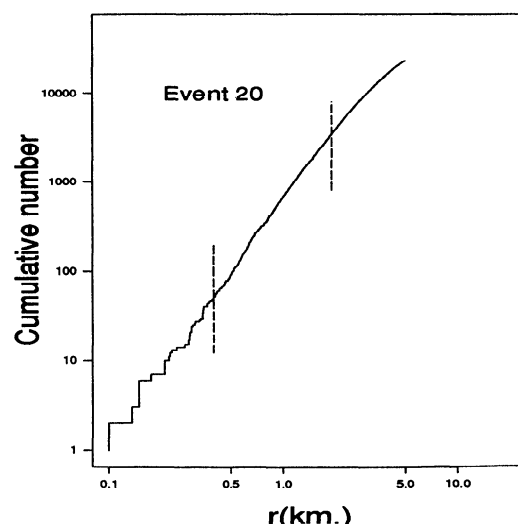


**Figure 5.** Cumulative number of pairs of hypocenters whose three-dimension distances are smaller than  $r$ ,  $N(r)$ , versus distance of pair hypocenters of aftershocks of event 20. The vertical bars show the range of fitted distances.

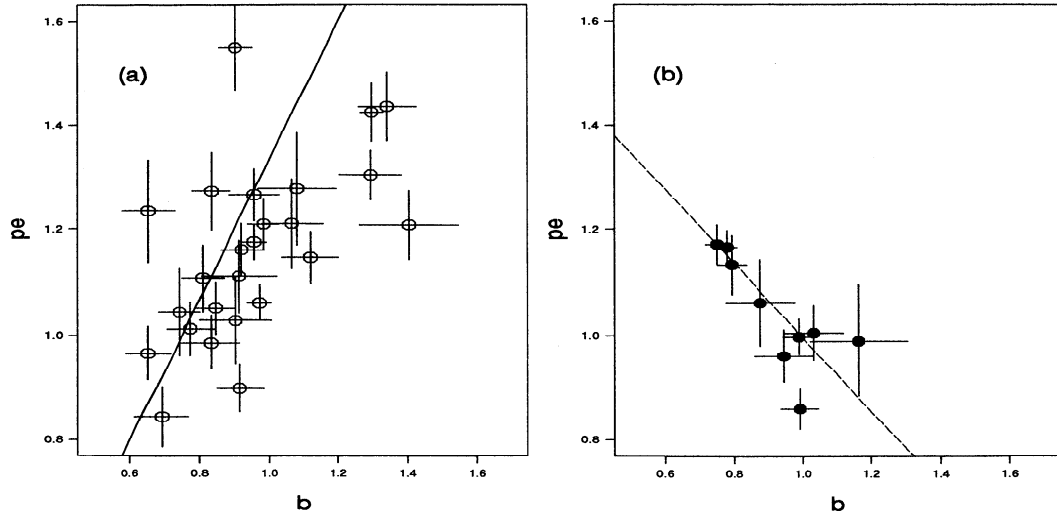


**Figure 6.** Scatterplots of  $\hat{p}_e$  versus  $\hat{b}$  value of the Gutenberg and Richter [1954] relation for (a) intraplate earthquakes and (b) interplate earthquakes. The horizontal and vertical bars show the corresponding estimated standard errors. The solid and dashed lines are described in the text.

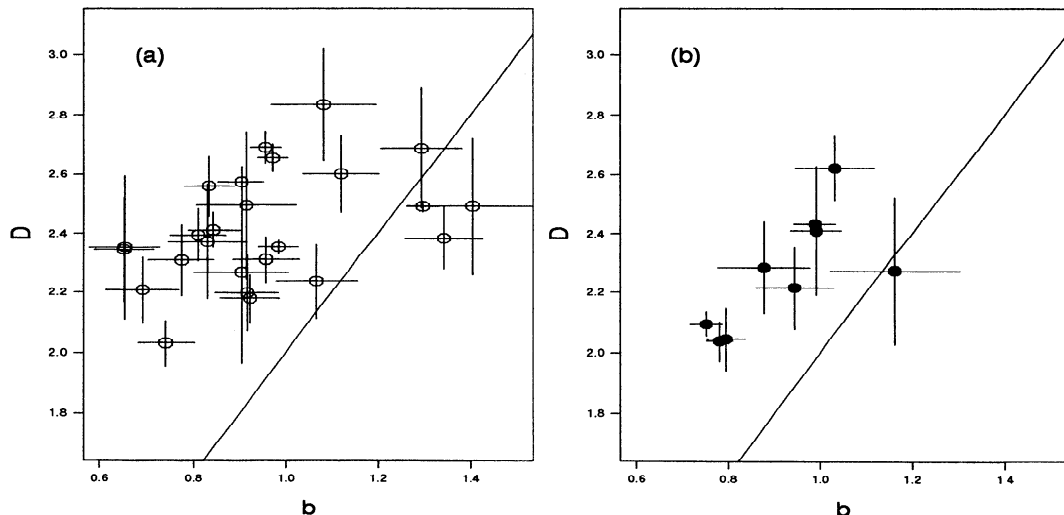
nitude  $M \geq 5$  in a wide region off the east coast of the Tohoku region of Japan over the time period 1926 through 1986, showed that the time series of  $\hat{b}$  and  $\hat{D}$  have a negative crosscorrelation of the time lag zero. A similar result was obtained by Henderson *et al.* [1992] for seismicity in southern California during 1970–1990. However, their area and time span for estimating  $\hat{b}$  and  $\hat{D}$  are too wide and too long, respectively, to examine the relation of the two quantities; opposite trends in the moving averaged time series of  $\hat{b}$  and  $\hat{D}$  can lead to a seeming negative correlation between them, while our  $(\hat{b}, \hat{D})$  plot is based on independent samples taken from distinct periods and regions.

The scatterplot in Figure 8a shows a clear positive correlation between  $\hat{p}_e$  and  $\hat{D}$  for intraplate earthquakes, and the estimated slope (dashed line) of the scatterplot is 1.294 using principal component analysis.

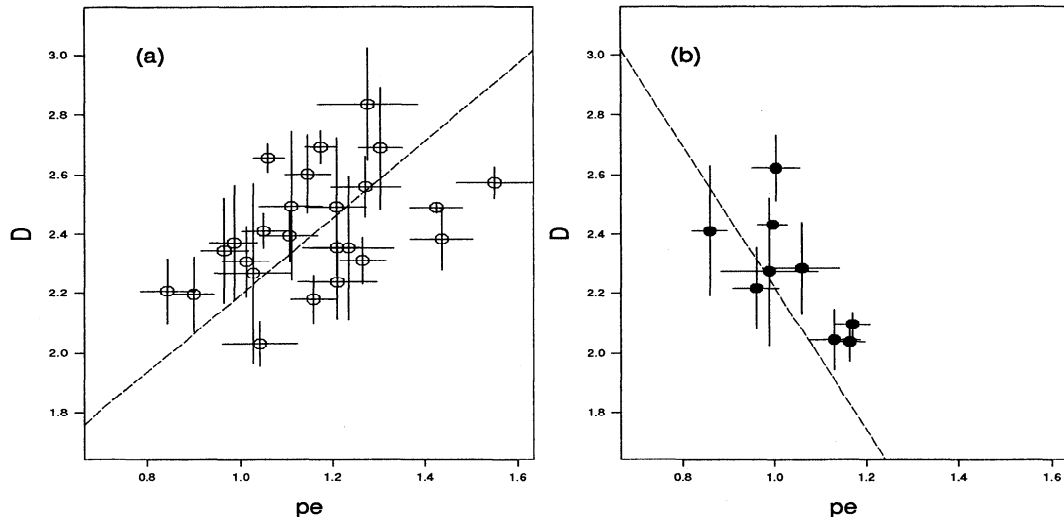
On the other hand, Figure 8b shows a clear negative correlation between  $\hat{p}_e$  and  $\hat{D}$  for interplate earthquakes with an estimated slope (dashed line) of -2.382. The results for intraplate events are consistent with those of Guo and Ogata [1995], who estimated the  $p$  value by the modified Omori formula and also estimated the fractal dimension  $D$  by least squares.

Figure 9a shows a clear negative correlation between  $\hat{\alpha}$  and  $\hat{b}$  for intraplate earthquakes, with an estimated slope (dashed line) of -0.155 using principal component analysis. On the other hand, a clear positive correlation is seen between  $\hat{\alpha}$  and  $\hat{b}$  for interplate events in Figure 9b, with an estimated slope (dashed line) of 0.083 from principal component analysis.

Similar contrasting correlations between  $\hat{\alpha}$  and  $\hat{D}$  for intraplate and interplate earthquakes are also shown in Figures 10a and 10b, respectively. The estimated



**Figure 7.** Scatterplots of the MLEs of the fractal dimension,  $\hat{D}$ , versus  $\hat{b}$  for (a) intraplate earthquakes and (b) interplate earthquakes. The horizontal and vertical bars show the corresponding estimated standard errors. The solid and dashed lines are described in the text.



**Figure 8.** Scatterplots of  $\hat{D}$  versus  $\hat{p}_e$  for (a) intraplate earthquakes and (b) interplate earthquakes. The horizontal and vertical bars show the corresponding estimated standard errors. The dashed lines are described in the text.

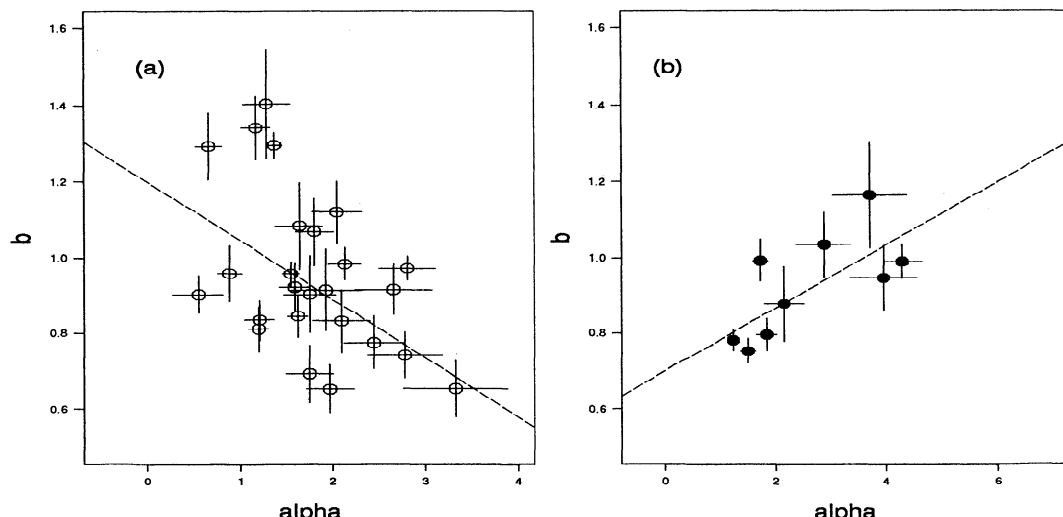
slopes (dashed lines) from principal component analysis for intraplate and interplate earthquakes are  $-0.104$  and  $0.082$ , respectively.

## Discussion

The slip on the fault plane varies considerably, and aftershocks' density in space appears negatively correlated with the slip [e.g., *Das and Aki, 1977; Takeo, 1987; Hartzell, 1989; Beroza, 1991*]. Therefore distribution of aftershocks in time, space, and magnitude may reflect such dynamics and geometry of fault surfaces, heterogeneity in frictional strength, and related physical environments, such as temperature and pore pressure [*Mogi, 1962b; Scholz, 1968; Kisslinger and Jones, 1991*;

*Aviles and Scholz, 1987*]. Figures 6-10 and Table 4 show the contrasting correlation patterns between the statistical parameters for the intraplate earthquakes and interplate earthquakes except for the case between the fractal dimension  $D$  and the  $b$  value. These may reflect some intrinsically different features in rupturing process between earthquakes within a plate and on an interface between two plates, as mentioned in the Introduction.

In particular, the implications of the contrast in  $(\hat{b}, \hat{p}_e)$  patterns in Figures 6a and 6b appear substantial enough to start our discussion. First, our scatterplot for intraplate aftershocks in Figure 6a is clearly positively correlated and is also consistent with *Utsu's* [1961] relation  $p = 4b/3$ . It is surmised that these parameters for the intraplate events are mainly affected by the tem-



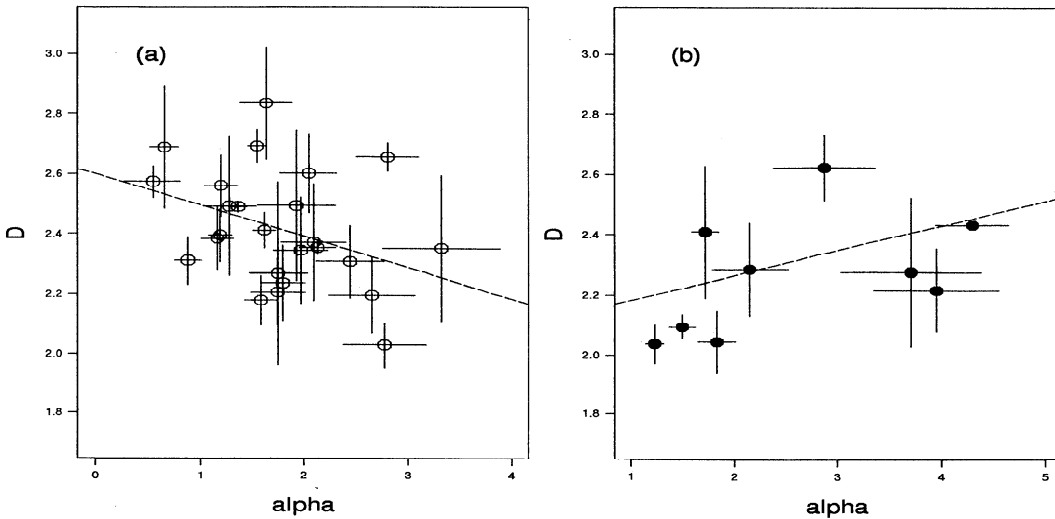


**Figure 10.** Scatterplots of  $\hat{D}$  versus  $\hat{\alpha}$  for (a) intraplate earthquakes and (b) interplate earthquakes. The horizontal and vertical bars show the corresponding standard errors. The dashed lines are described in the text.

perature. In fact, *Mogi* [1967] and *Kisslinger and Jones* [1991] suggest that  $p$  is positively correlated with heat flow and interpret that the residual stress at the aftershock region relaxes rapidly in a high-temperature environment as does the decay of aftershocks. In our data, many shallow intraplate events with high  $p$  value relate to volcanic activity, which also tends to provide larger  $b$  values and smaller  $\alpha$  values, as seen in Figures 4 and 6a. At the same time, one of the delayed fracture models suggested by *Yamashita and Knopoff* [1987] assumes inverse power law distribution for the barrier sizes to derive the modified Omori law with  $p=1.0\text{--}1.3$ , also leading to a positive correlation with  $b$  value. This model appears to be related to the fractal (self-similar) features of the barriers in fault surfaces.

However, these relations are not consistent with the simulation result of a frictional fault model by *Mikumo and Miyatake* [1979]; that is, negative correlation between  $p$  and  $b$  holds, which is now consistent with the result in Figure 6b for the interplate events. Since the depth of the interplate earthquakes along thrust zone reaches about 60 km, we tested the possible relation of each parameter to hypocentral depth of the mainshock. Table 5 summarizes the significance of such correlations. The observed correlations of the parameters for interplate aftershocks are high and significant, in spite of the small number of the events, while no such remarkable correlations were found for the intraplate events. In particular, correlations of  $\hat{p}$  and  $\hat{b}$  to the depth are very clearly negative and positive, respectively, as shown in Figure 11. The fitted lines by linear regression are  $\hat{p}_e = -0.0043h + 1.16$  and  $b = 0.0053h + 0.78$ . On the other hand, for intraplate cases, the parameters are much scattered against depth with a similar range between about 0 and 60 km. These are very important in understanding the correlations between parameters for plate boundaries.

Some geological studies of accretionary wedges in fossil subduction zones, cited by *Scholz* [1990, section 6.3.2], suggest that temperature along the thrust zone is not very sensitive to depth, but, instead, the pore pressure should increase with depth, weakening basal friction against the increasing pressure in depth. These observations lead us to think that heterogeneity of static frictional strength in the sense of *Mikumo and Miyatake* [1979] might increase as the increasing inhomogeneous pore pressure with depth along subducted slab. Indeed, they simulated a frictional fault model with random distributions of static frictional strength and relaxation times to realize both the Gutenberg-Richter rela-

**Table 5.** Correlations Between Parameters and Depth

Correlation	$\rho$	$\Lambda$	$Z_n$	Confidence	Slope ( $km^{-1}$ )
<i>Intraplate, n=25</i>					
$\hat{p}_e, h$	-0.074	0.1	0.347	no	
$\hat{b}, h$	-0.105	0.3	0.496	no	
$\hat{\alpha}, h$	0.388	4.1	1.922	weak	0.0153
$\hat{D}, h$	-0.093	0.2	0.436	no	
<i>Interplate, n=9</i>					
$\hat{p}_e, h$	-0.909	15.8	3.730	clear	-0.0043
$\hat{b}, h$	0.845	11.3	3.033	clear	0.0053
$\hat{\alpha}, h$	0.668	5.3	1.978	clear	0.0355
$\hat{D}, h$	0.648	4.9	1.890	weak	0.0059

Definitions are same as in Table 4. Here  $h$  is the depth of main shock. Slopes here are estimated by the linear regression.

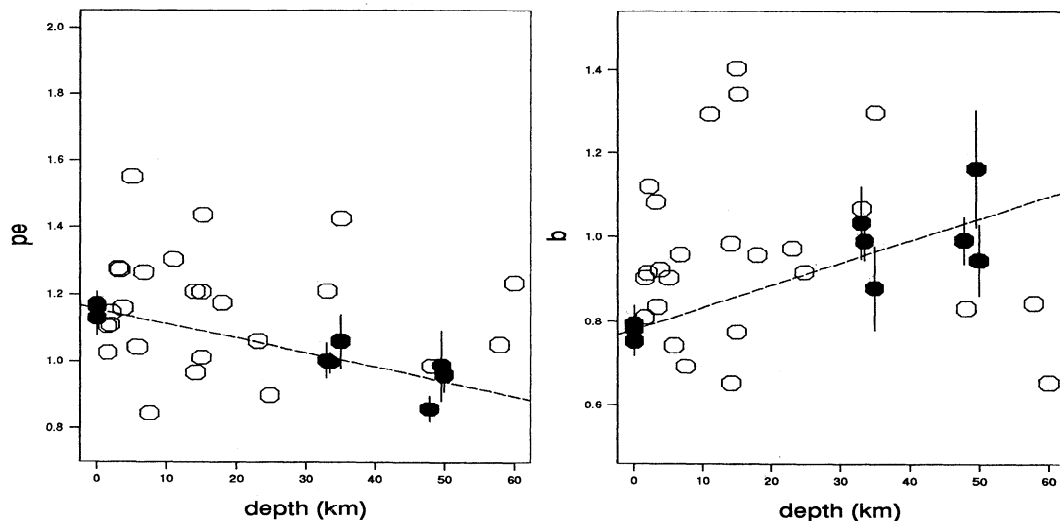


**Figure 11.** Scatterplots of  $\hat{b}$  and  $\hat{p}_e$  versus the depth of the main shocks, respectively. Open and solid circles indicating those of intraplate and interplate earthquakes, respectively. The dashed lines are described in the text.

tion and the modified Omori relation for aftershocks. Among experiments under the various combinations of adjusting parameters, of particular importance is the following comparison between two typical experiments. The first experiment has larger variability in the distribution of static frictional strength than the second, which results in smaller  $p$  and larger  $b$ . Further comparisons with other experiments suggest that  $p$  is insensitive to the variability of relaxation times. Our interplate earthquake result in Figure 11 (which implies the negative correlation in Figure 6b) might support the above speculation. Further, the somewhat similar effect on  $D$  and  $\alpha$  as increasing depth is surmised from the significance of the statistics in Table 5.

Mikumo and Miyatake [1979] also describe in their experiments that the stress drop of the second experiment is significantly large (exceeding 15 MPa) compared with the first one (of the order of 2–3 MPa), while the higher stress drop gives a lower  $b$  value. This result also reminds us of the important dynamical contrast in stress drop between the intraplate and interplate types of ruptures [Kanamori and Anderson, 1975; Scholz *et al.*, 1986]. That is, the degree of heterogeneity of frictional strengths may be essential to discriminate the two types of aftershocks. Figures 7a and 7b, although both similar in positive correlation, show that  $b$  values for intraplate events distribute smaller than those for plate boundary events for a fixed fractal dimension  $D$ ; that is,  $\hat{b} - \hat{D}/2$  for intraplate events, on average, is smaller than that for interplate events. On the other hand, Figures 7a and 7b show that the range of the fractal dimensions  $D$  of interplate aftershocks appears about the same as that in the plate boundary, which suggests that the complexity in the faults may not be very different from each other.

Another well-known empirical observation of aftershocks in thrust zones is the diffusion of aftershock activity often seen in large interplate earthquakes [Mogi,

1968], which is reduced to rather homogeneous distribution of smaller asperities in the focal zone [Tajima and Kanamori, 1985]. The gradual diffusion of aftershock activity in space may relate to our observation of the low  $p$  ( $\approx 1.0$ ) and its small variability, along with the larger  $\alpha$  for interplate aftershocks (see Figures 2 and 4). It should be noted, in comparison with slopes in Figures 8a and 8b, that  $p_e$  for intraplate events is more sensitive to the fractal dimension  $D$ , whose ranges for both types are similar to each other.

To summarize our speculation, the contrasting correlations of parameters could be reduced to the following scheme. The aftershock parameters for intraplate events are mainly affected by temperature (heat flow of the area) or structural heterogeneity (inverse power distribution of barrier sizes), while those of interplate events are mainly affected by depth. That is, in thrust zones, the degree of inhomogeneity of pore pressure surpasses the change of temperature in affecting heterogeneity of frictional strength of the interface. All the parameters, except fractal dimension  $D$ , change with temperature within a plate, while all the parameters, except  $p$  value, increase with depth on a plate boundary. Regardless of the type of events,  $p$  decreases and  $\alpha$  increases, as heterogeneity of frictional strength increases.

## Conclusions

For the majority of the aftershock sequences, the ETAS model is preferred by AIC to the nonstationary Poisson process model of the modified Omori formulas, which suggests existence of clusters within the aftershock sequence. The  $\hat{p}_e$  value of the ETAS is about equal to or larger than the conventional  $\hat{p}_o$  value for the same data. In particular,  $\hat{p}_o$  and  $\hat{p}_e$  are almost equal to each other and  $\hat{\alpha}$  takes large value when the modified Omori model is preferred by AIC.

The  $\hat{p}_e$  has values around 1.0 with small variability for interplate events, while it has higher values with large variability for intraplate earthquakes. Most  $\hat{\alpha}$  values of the ETAS are smaller than 2.0 for intraplate earthquakes, while they are larger than 1.0 interplate events.

Our results concerning the correlations between the statistical parameters of the aftershocks in time ( $\alpha$  and  $p$  value), space (fractal dimension  $D$  of hypocenter distribution) and magnitude ( $b$  value) are summarized as follows.

1. The correlation between the estimated  $\hat{\alpha}$  and  $\hat{p}_e$  is negative for both intraplate and interplate earthquakes. The slopes of fitted lines are significantly different between the intraplate and interplate events.

2. Positive correlations between all pairs of  $\hat{b}$ ,  $\hat{p}_e$ , and  $\hat{D}$  for intraplate earthquakes are seen, and a plot of the pairs  $(\hat{b}, \hat{p}_e)$  is well superimposed by Utsu's relation  $p = 4b/3$ . Negative correlations are seen for pairs  $(\hat{b}, \hat{p}_e)$  and  $(\hat{p}_e, \hat{D})$  for interplate earthquakes.

3. Pairs  $(\hat{b}, \hat{D})$  for interplate events have a positive correlation similar to those for the intraplate events, and both slopes are consistent with Aki's relation  $D = 2b$ , where  $D$  is the fractal dimension of faults' configuration. However, the bias of the intersect  $\hat{D} - 2\hat{b}$  for intraplate events is systematically larger than that for interplate events.

4. Scatterplots of  $(\hat{\alpha}, \hat{b})$  and  $(\hat{\alpha}, \hat{D})$  for intraplate earthquakes showed negative correlations, while  $(\hat{\alpha}, \hat{b})$  and  $(\hat{\alpha}, \hat{D})$  for interplate earthquakes showed positive correlations.

5. The correlations of the parameters and depth are high and significant for interplate earthquakes but are negligible for intraplate earthquakes.

## Appendix: Statistical Methods

### Relation of Palm Intensity to Autocovariance

Consider a point process in three-dimensional space with a vector denoted by  $\mathbf{r} = (x, y, z)$  in Cartesian coordinates and  $(r, \vartheta, \varphi)$  in polar coordinates. Let  $N(d\mathbf{r})$  be the number of events in a volume  $d\mathbf{r} = dx dy dz = r^2 dr sin \vartheta d\vartheta d\varphi$ . Here we assume stationarity of the probability law with respect to any location shift of a set of points. The covariance density  $c(\cdot)$  of the point process  $N(\cdot)$  is such that

$$\text{cov}[N(d\mathbf{r}), N(d\mathbf{r}')] = c(\mathbf{r} - \mathbf{r}') d\mathbf{r} d\mathbf{r}', \quad (12)$$

for a pair of points  $\mathbf{r}$  and  $\mathbf{r}'$ ,  $\mathbf{r} \neq \mathbf{r}'$ . The Palm intensity  $\lambda_o(\cdot)$  is given by

$$\begin{aligned} \lambda_o(\xi) d\xi &\equiv \Pr[N(d\xi) \geq 1 | N(\mathbf{o}) = 1] \\ &= E[N(d\xi) | N(\mathbf{o}) = 1], \end{aligned} \quad (13)$$

for the conditional occurrence rate at location,  $\xi$  given that an event occurred at the origin  $\mathbf{o}$ . Then, the left-hand side of (12) is equal to

$$\begin{aligned} E[N(d\mathbf{r})N(d\mathbf{r}')] - \mu^2 d\mathbf{r} d\mathbf{r}' \\ = [\mu \lambda_o(\mathbf{r} - \mathbf{r}') - \mu^2] d\mathbf{r} d\mathbf{r}', \end{aligned} \quad (14)$$

owing to the definition of the Palm intensity. Thus, for  $\xi = \mathbf{r} - \mathbf{r}'$ , the Palm intensity is

$$\lambda_o(\xi) = \mu + \frac{c(\xi)}{\mu}, \quad \xi \neq \mathbf{0}, \quad (15)$$

from (12) and (14), where  $\mu$  is the average seismicity rate:  $E[N(d\mathbf{r})] = \mu d\mathbf{r}$ .

### Maximum Likelihood Estimates

We choose the parameters of the distribution for which the joint probability of the sample is a maximum. In the case of independent observations, the joint probability is proportional to the product of probability densities of each observation. For instance, the Gutenberg-Richter magnitude frequency law (1) lead to the exponential density distribution  $f(M; b) = (b \ln 10) \exp\{-b \ln 10(M - M_c + 0.05)\}$  for a cutoff magnitude  $M_c$ , where "ln" is the natural logarithm. Given a set of observed magnitudes  $\{M_i; i = 1, 2, \dots, N\}$ , the likelihood function  $L(b)$  is the function of the parameter  $b$  such that  $L(b) = \prod_{i=1}^N f(M_i; b)$ . In practice, we maximize the log likelihood  $l(b) = \ln L(b) = \sum_{i=1}^N \ln f(M_i; b)$  with respect to the parameter  $b$ , which led to the maximum likelihood estimate  $\hat{b}$  in (1).

The joint distributions to define the likelihood can be general, and the maximum likelihood estimate (MLE) is obtained simply by maximizing the log likelihood function  $l(\theta)$  with respect to the parameters  $\theta$ . Mostly, the maximization is implemented numerically by using a nonlinear optimization algorithm.

The likelihood function of a point process is expressed in terms of the intensity function  $\lambda_\theta(t)$ . Given an observed sequence of aftershock occurrence times and magnitudes  $\{(t_i, M_i); i = 1, 2, \dots, N\}$  in the time interval  $(S, T)$ , MLEs of the parameters for the models in (4), (5), and (8) are given by maximizing the log likelihood function

$$l(\theta) = \sum_{i=1}^N \ln \lambda_\theta(t_i) - \int_S^T \lambda_\theta(t) dt \quad (16)$$

with respect to parameters  $\theta$ , and their estimated standard errors can be found using the Hessian matrix as described in the next section. The explicit form of the log likelihood (16) for the modified Omori functions (3) and (4) are given by Ogata [1983], and the one for the ETAS model is given by Ogata [1988],

Let  $\mathbf{r}_1, \mathbf{r}_2, \dots, \mathbf{r}_n$  be locations of events in some three-dimensional volume, and consider the random set of vector differences of pairs  $\{\xi_{ij} = \mathbf{r}_i - \mathbf{r}_j; i = 1, 2, \dots, n; i < j\}$ . This is a set of points centered at the origin of the Palm intensity  $\lambda_o(\cdot)$ . Such a superposed point pattern  $\{\xi_{ij}\}$  for some annular domain is usually well approximated by a nonhomogeneous Poisson process, so that dependence among the random points  $\{\xi_{ij}\}$  can be neglected. Given a set of such vectors  $\{\xi_{ij} = \mathbf{r}_i - \mathbf{r}_j; i, j = 1, 2, \dots, n; i < j\}$  on a suitable annular region,  $A(\varepsilon, R) = \{\xi = (r, \vartheta, \varphi); \varepsilon \leq r \leq R\}$ , the log likelihood function for the Palm intensity model in (15) is

$$l = \sum_{i < j} \ln \lambda_o(\xi_{ij}) - \int \int \int_{A(\varepsilon, R)} \lambda_o(\xi) d\xi, \quad (17)$$

where the sum is taken over all ordered pairs  $i$  and  $j$  such that  $\xi_{ij} \in A(\varepsilon, R)$ . The log likelihood in (17) can then be expressed in polar coordinates:

$$\begin{aligned} l(\theta) &= \sum_{i < j} \ln \lambda_\theta(\mathbf{r}_{ij}) \\ &\quad - \int_\varepsilon^R \int_0^\pi \int_0^{2\pi} \lambda_\theta(\mathbf{r}) r^2 \sin \vartheta dr d\vartheta d\varphi \\ &= \sum_{i < j} \ln \left( \mu + \frac{K}{r_{ij}^H} \right) - \frac{4\pi\mu}{3} (R^3 - \varepsilon^3) \\ &\quad - \frac{4\pi K}{3-H} (R^{3-H} - \varepsilon^{3-H}), \end{aligned} \quad (18)$$

where the sum is taken over all  $\mathbf{r}_{ij}$ , with  $|\mathbf{r}_{ij}|$  between  $\varepsilon$  and  $R$ . The maximum likelihood estimates  $\hat{\theta} = (\hat{\mu}, \hat{K}, \hat{H})$  are obtained by maximizing the log likelihood function in (18), and their estimated standard errors can be found using the Hessian matrix as described in the next section.

### Estimation Errors

The maximum likelihood method also admits estimates of the variance and covariance of the errors in the estimated parameters. For example, consider the MLEs, say,  $\hat{\theta} = (\hat{\mu}, \hat{K}_0, \hat{c}, \hat{\alpha}, \hat{p}_e) = (\hat{\theta}_1, \hat{\theta}_2, \hat{\theta}_3, \hat{\theta}_4, \hat{\theta}_5)$ , of the ETAS model. The log likelihood function in (16) around  $\hat{\theta}$  is approximately given by the quadratic function

$$l(\theta) = l(\hat{\theta}) - \frac{1}{2}(\theta - \hat{\theta}) J(\hat{\theta})(\theta - \hat{\theta})^T, \quad (19)$$

using Taylor's expansion formula, where

$$J(\hat{\theta}) = -\left(\frac{\partial^2 l(\hat{\theta})}{\partial \theta_i \partial \theta_j}\right), \quad i, j = 1, 2, \dots, 5, \quad (20)$$

is called the Hessian matrix. On the basis of the standard, large-sample theory, the joint estimation errors of the MLE  $\hat{\theta}$  are approximately distributed according to a normal distribution  $N(\hat{\theta}, S(\hat{\theta}))$ , where the covariance matrix  $S(\hat{\theta}) = J(\hat{\theta})^{-1}$ . The standard errors for individual components of the MLEs are the square roots of the corresponding diagonal elements  $\hat{\sigma}_{ii}$  of the estimated covariance matrix  $S(\hat{\theta})$ .

In the case of the  $b$  value estimate in (2), we can easily derive  $S(b) = \hat{b}^2/N$ , which was given by Aki [1965]. Similarly, the error estimate of  $p$  and  $\alpha$  in (8) and also that of  $D$  are obtained from the corresponding component of the diagonal in the matrix  $S(\hat{\theta})$ . However, in general, off-diagonal components of the covariance matrix  $S(\hat{\theta}) = (\hat{\sigma}_{ij})$  are nonzero, which means that there is some correlation between the errors of  $\hat{\theta}_i$  and  $\hat{\theta}_j$ . For instance, consider the two parameters  $\alpha$  and  $p_e$  in the ETAS model. The expected correlation of the errors between the MLE of  $\alpha$  and  $p_e$  is  $\hat{\rho} = \hat{\sigma}_{\alpha p_e} / \sqrt{\hat{\sigma}_\alpha \hat{\sigma}_{p_e}}$ , where  $\hat{\sigma}_{\alpha p_e} = \hat{\sigma}_{35}$ ,  $\hat{\sigma}_\alpha = \hat{\sigma}_{33}$ , and  $\hat{\sigma}_{p_e} = \hat{\sigma}_{55}$ ; the joint standard error ellipsoid shown in Figure 4 is such that

$$\frac{1}{1 - \hat{\rho}^2} \left\{ \left( \frac{\alpha - \hat{\alpha}}{\hat{\sigma}_\alpha} \right)^2 - 2\hat{\rho} \left( \frac{\alpha - \hat{\alpha}}{\hat{\sigma}_\alpha} \right) \left( \frac{p - \hat{p}_e}{\hat{\sigma}_{p_e}} \right) + \left( \frac{p_e - \hat{p}_e}{\hat{\sigma}_{p_e}} \right)^2 \right\} = 1. \quad (21)$$

### Model Selection

The Akaike information criterion [Akaike, 1974] provides a consistent way for selecting among competing models fitted by maximum likelihood and is defined by

$$\begin{aligned} \text{AIC} &= (-2) \max \log \text{likelihood} \\ &\quad + 2 \times (\text{number of fitted parameters}) \\ &= (-2) \max_\theta l(\theta) + 2 \dim(\theta), \end{aligned} \quad (22)$$

where the maximum of the log likelihood function  $l(\theta)$  is attained with respect to the parameters  $\theta$ . AIC trades off fit to the data and model complexity. A model with a smaller AIC value is considered to be preferable.

When one of the two models is included appropriately in the other one, we can use the conventional likelihood ratio test. It is useful to note that the log likelihood ratio test statistic is related to the AIC by

$$\begin{aligned} \Lambda &= (-2)\{\hat{l}(H_0) - \hat{l}(H_1)\} \\ &= \text{AIC}(H_0) - \text{AIC}(H_1) + 2k, \end{aligned} \quad (23)$$

where the model  $H_1$  contains the model  $H_0$  as a restricted family,  $k$  denotes the difference of dimensions of parameters in  $H_0$  and  $H_1$ , and  $\Lambda$  has the  $\chi_k^2$  distribution under the null hypothesis  $H_0$ . The comparison of the minimum AIC procedure with the conventional likelihood ratio test procedure is discussed by Akaike [1977, 1983].

For the correlations between the characteristic parameters in the text, we assume that pairs of variables  $(X, Y) = \{(x_i, y_i); i = 1, 2, \dots, n\}$  obey a bivariate normal distribution. We consider two hypotheses. The null hypothesis  $H_0$  assumes that the correlation  $\rho_0 = 0$ , and so it has four free parameters with MLEs  $\hat{\theta} = (\bar{x}, \bar{y}, \hat{\sigma}_x^2, \hat{\sigma}_y^2)$ , where  $\bar{x}$  and  $\bar{y}$  are the sample means and  $\hat{\sigma}_x^2$  and  $\hat{\sigma}_y^2$  are the sample variances. The alternative hypothesis  $H_1$  assumes that the correlation  $\rho \neq 0$ , and so it has five free parameters with MLEs  $\hat{\theta} = (\bar{x}, \bar{y}, \hat{\sigma}_x^2, \hat{\sigma}_y^2, \hat{\rho})$ , where  $\hat{\rho}$  is the sample correlation. The AIC values for the two models are

$$\text{AIC}(H_0) = 2n \ln(\hat{\sigma}_x \hat{\sigma}_y) + 2 \times 4, \quad (24)$$

$$\text{AIC}(H_1) = 2n \ln\{\hat{\sigma}_x \hat{\sigma}_y \sqrt{1 - \hat{\rho}^2}\} + 2 \times 5. \quad (25)$$

If  $\text{AIC}(H_1) < \text{AIC}(H_0)$ , which corresponds to  $\Lambda > 2.0$ , this suggests the preference of the nonzero correlation between the variables  $X$  and  $Y$ .

However, the conventional likelihood ratio test cannot be directly applied to test the modified Omori formula (4) against the ETAS model (8). Although the set of parameters  $(\mu, K_0, c, \alpha, p_e)$  formally includes  $(K, c, p_o)$ ,  $\alpha$  does not satisfy the regularity condition for the standard, large-sample theory, such as the likelihood ratio statistic being chi-square distributed (while

$\mu$  does), because we get the Omori function from the ETAS by setting  $\mu = 0$  but  $\alpha \uparrow \infty$ . That is, when the ETAS is fitted to the aftershock sequence, which is very near to Poisson with the modified Omori formula, the MLE  $\hat{\alpha}$  gets very large while  $\hat{K}_0$  gets very small. On the other hand, the extended version of the Omori formula (5) satisfies the regularity condition to test (4) against this, but apparently, the model (5) cannot be tested against the ETAS. Therefore we used AIC for comparison of these models.

### Residual Analysis for Point Processes

Residual analysis of points process data [Ogata, 1988, 1989, 1992] is also useful to examine whether the major features of the given data can be reproduced by the estimated models. Suppose that the point process  $\{t_i\}$  are generated by the intensity function  $\lambda(t)$ . Consider the integral of the intensity

$$\Lambda(t) = \int_S^T \lambda(t) dt, \quad (26)$$

which is a monotonically increasing function because  $\lambda(t)$  is nonnegative. If we consider the random time change  $\tau = \Lambda(t)$  from  $t$  to  $\tau$ , then  $\{t_i\}$  is transformed one to one into  $\{\tau_i\}$ . It is well known that  $\{\tau_i\}$  has the distribution of stationary Poisson process of intensity 1. Therefore, if the estimated intensity  $\lambda_{\hat{\beta}}(t)$  is a good approximation to the true  $\lambda(t)$ , then the transformed data  $\{\tau_i\}$  from the real data are expected to behave like a stationary Poisson process. Figures 3a and 3b show the plot of the cumulative number of points  $\{\tau_i\}$  versus transformed time  $\tau = \Lambda(t)$  of the aftershocks of event 10 for the modified Omori formula and the ETAS model, respectively. We can see in this case that the ETAS model fits better than the modified Omori formula.

Another possible test of the data against the modified Omori function could be carried out by comparing the present, parametrically estimated Omori curve (4) with nonparametrically estimated envelopes, except assuming the monotonically decreasing trend [Hengartner and Stark, 1995].

### Principal Component Analysis

Suppose that pairs of variables  $(X, Y) = \{(x_i, y_i); i = 1, 2, \dots, n\}$  are given. It should be noted that in both the linear regression  $y_i = ax_i + b + \epsilon_i$  and  $x_i = cy_i + d + \eta_i$ , we assume a noise for only one of the variables. Thus, in the plot of  $y$  versus  $x$ , the slopes  $a$  and  $1/c$  can be different from each other. One the other hand, the linear fit by the principal component analysis assumes that the both of the pairs have their noises of the same variance and independent of each other. Assume that averages of both variables are equal to zero without loss of generality, then the slope of  $y$  versus  $x$  axis ( $v/u$ ) is obtained by minimizing  $\sum_i (ux_i + vy_i)^2$  under the restriction of  $u^2 + v^2 = 1$  (see Kendall [1957], for instance, for more general settings).

**Acknowledgments.** We would like to thank Tokuji Utsu for the useful discussions on the subject and suggestions of related references. We are also very grateful to Philip Stark, David Steinberg, and David Vere-Jones for their constructive comments which significantly improved our manuscript. We used SEIS-PC [Ishikawa et al., 1985] for the hypocenter data visualization. The present study was partially supported by a Grant-in-Aid for Scientific Research (C) from the Ministry of Education, Science, Sport and Culture.

### References

- Akaike, H., A new look at the statistical model identification, *IEEE Trans. Autom. Control*, **AC-19**, 716-723, 1974.
- Akaike, H., On entropy maximization principles, in *Applications of Statistics*, edited by P. R. Krishnaiah, pp. 27-41, North-Holland, New York, 1977.
- Akaike, H., Information measure and model selection, *Bull. Int. Statist. Inst.*, **50**, 277-290, 1983.
- Aki, K., Maximum likelihood estimate of  $b$  in the formula  $\log N = a - bm$  and its confidence, *Bull. Earthquake Res. Inst. Univ., Tokyo*, **43**, 237-239, 1965.
- Aki, K., A probabilistic synthesis of precursory phenomena, in *Earthquake Prediction: An International Review*, Maurice Ewing, Ser., vol.4, edited by D.W. Simpson and P.G. Richards, pp. 566-574, AGU, Washington, D.C., 1981.
- Aviles, C. A., and C. H. Scholz, Fractal analysis applied to characteristic segments of the San Andreas Fault, *J. Geophys. Res.*, **92**, 331-344, 1987.
- Bak, P., and C. Tang, Earthquakes as a self-organized critical phenomenon, *J. Geophys. Res.*, **94**, 15,635-15,637, 1989.
- Beroza, G., Near-source modeling of the Loma Prieta earthquake: Evidence for heterogeneous slip and implications for earthquake hazard, *Bull. Seismol. Soc. Am.*, **81**, 1603-1621, 1991.
- Das, S., and K. Aki, Fault plane with barriers: A versatile earthquake model, *J. Geophys. Res.*, **82**, 5658-5670, 1977.
- Grassberger, P., Generalized dimensions of strange attractors, *Phys. Lett. A*, **97**, 227-230, 1983.
- Guo, Z., and Y. Ogata, Correlation between characteristic parameters of aftershock distributions in time, space and magnitude, *Geophys. Res. Lett.*, **22**, 993-996, 1995.
- Gutenberg, B., and C. F. Richter, *Sismicity of the Earth*, 310 pp., Princeton Univ. Press, Princeton, N. J., 1954.
- Hartzell, S., Comparison of seismic waveform inversion results for the rupture history of a finite fault: Application to the 1986 North Palm Springs, California, earthquake, *J. Geophys. Res.*, **94**, 7515-7534, 1989.
- Henderson, J., I. G. Main, P. G. Meredith, and P. R. Sammonds, The evolution of seismicity-observation, experiment and a fracture-mechanical interpretation, *J. Struct. Geol.*, **14**, 905-913, 1992.
- Hengartner, N. W., and P. B. Stark, Finite-sample confidence envelopes for shape-restricted densities, *Ann. Stat.*, **23**, 525-550, 1995.
- Hirata, T., Omori's power law for aftershocks and fractal geometry of multiscale fault system (in Japanese), *J. Seismol. Soc. Jpn.*, **39**, 478-481, 1986.
- Hirata, T., A correlation between the  $b$  value and the fractal dimension of earthquakes, *J. Geophys. Res.*, **94**, 7505-7514, 1989.
- Ishikawa, Y., K. Matsumura, H. Yokoyama, and H. Matsumoto, Development of SEIS-PC: A summary (in Japanese), *J. Struct. Geol.*, **19**, 19-27, 1985.
- Ito, K., and M. Matsuzaki, Earthquakes as self-organized critical phenomena, *J. Geophys. Res.*, **95**, 6853-6860, 1990.

- Kagan, Y. Y., and L. Knopoff, Spatial distribution of earthquakes: The two-point correlation function, *Geophys. J. R. Astron. Soc.*, 62, 303-320, 1980.
- Kanamori, H., and D. L. Anderson, Theoretical basis of some empirical relations in seismology, *Bull. Seismol. Soc. Am.*, 65, 1073-1095, 1975.
- Kendall, M. G., *A Course in Multivariate Analysis*, Charles Griffin, London, 1957.
- Kikuchi, M., and H. Kanamori, Source process of the 1994 Hokkaido-Toho-Oki earthquake, paper presented at Japan Earth and Planetary Science Joint Meeting, Seismol. Soc. Jpn., Osaka, 1995.
- King, G., The accommodation of large strains in the upper lithosphere of the earth and other solids by self-similar fault system: The geometrical origin of  $b$ -value, *Pure Appl. Geophys.*, 121, 761-815, 1983.
- Kisslinger, C., and L. M. Jones, Properties of aftershocks in southern California, *J. Geophys. Res.*, 96, 11,947-11,958, 1991.
- Main, I. G., Damage mechanics with long-range interactions: Correlation between the seismic  $b$ -value and the fractal two-point correlation dimension, *Geophys. J. Int.*, 111, 531-541, 1992.
- Mandelbrot, B. B., *The Fractal Geometry of Nature*, 468 pp., W.H. Freeman, New York, 1982.
- Matsu'ura, R. S., Detailed study of the earthquake sequence in 1980 off the east coast of the Izu peninsula, Japan, *J. Phys. Earth*, 31, 65-101, 1983.
- Matsu'ura, R. S., I. Karakama, and K. Tsumura, *List of Earthquakes in the Kanto Area and its Vicinity*, part 1, 578 pp., Earthquake Res. Inst., Univ. of Tokyo, Tokyo, 1988a.
- Matsu'ura, R. S., I. Karakama, and K. Tsumura, *List of Earthquakes in the Kanto Area and its Vicinity*, part 2, 562 pp., Earthquake Res. Inst., Univ. of Tokyo, Tokyo, 1988b.
- Matsuzaki, M., and H. Takayasu, Fractal features of the earthquake phenomenon and a simple mechanical model, *J. Geophys. Res.*, 96, 19,925-19,931, 1991.
- Mikumo, T., and T. Miyatake, Earthquake sequences on a frictional fault model with non-uniform strengths and relaxation times, *Geophys. J. R. Astron. Soc.*, 59, 497-522, 1979.
- Mogi, K., Study of the elastic shocks caused by the fracture of heterogeneous materials and its relation to the earthquake phenomena, *Bull. Earthquake Res. Inst. Univ. Tokyo*, 40, 125-173, 1962a.
- Mogi, K., On the time distribution of aftershocks accompanying the recent major earthquakes in and near Japan, *Bull. Earthquake Res. Inst. Univ. Tokyo*, 40, 107-124, 1962b.
- Mogi, K., Regional variation of aftershock activity, *Bull. Earthquake Res. Inst. Univ. Tokyo*, 45, 711-726, 1967.
- Mogi, K., Development of aftershock areas of great earthquakes, *Bull. Earthquake Res. Inst. Univ. Tokyo*, 46, 175-203, 1968.
- Ogata, Y., Estimation of the parameters in the modified Omori formula for aftershock frequencies by maximum likelihood procedure, *J. Phys. Earth*, 31, 115-124, 1983.
- Ogata, Y., Statistical models for earthquake occurrences and residual analysis for point process, *JASA J. Am. Stat. Assoc.*, 83(401), 9-27, 1988.
- Ogata, Y., Statistical model for standard seismicity and detection of anomalies by residual analysis, *Tectonophysics*, 169, 159-174, 1989.
- Ogata, Y., Detection of precursory relative quiescence before great earthquakes through a statistical model, *J. Geophys. Res.*, 97, 19,845-19,871, 1992.
- Ogata, Y., and K. Katsura, maximum likelihood estimates of the fractal dimension for random spatial patterns, *Biometrika*, 87, 463-474, 1991.
- Ogata, Y., and K. Shimazaki, Transition from aftershock to normal activity: the 1965 Rat Islands earthquake aftershock sequence, *Bull. Seismol. Soc. Am.*, 74, 1757-1765, 1984.
- Okada, Y., Chibaken-Toho-Oki Earthquake of December 17, 1987 (in Japanese), *Rep. 40*, pp. 81-86, Coord. Comm. for Earthquake Predict., Geogr. Surv. Inst., Minist. of Constr., Tsukuba, Japan, 1988.
- Omori, F., On the aftershocks of earthquakes, *J. Coll. Sci. Imp. Univ. Tokyo*, 7, 111-200, 1894.
- Sadovskiy, M.A., T.V. Golubeva, V.F. Pisarenko, and M.G. Shnirman, Characteristic dimensions of rock and hierarchical properties of seismicity, *Izv. Acad. Sci. USSR Phys. Solid Earth*, Engl. Transl., 20, 87-96, 1984.
- Scholz, C. H., The frequency magnitude of microfracturing in rock and its relation to earthquakes, *Bull. Seismol. Am.*, 58, 399-416, 1968.
- Scholz, C. H., *The Mechanics of Earthquakes and Faulting*, 439 pp., Cambridge Univ. Press, New York, 1990.
- Scholz, C. H., C. Aviles, and S. Wesnousky, Scaling differences between large intraplate and interplate earthquakes, *Bull. Seismol. Soc. Am.*, 76, 65-70, 1986.
- Tajima, F., and H. Kanamori, Global survey of aftershock area expansion patterns, *Phys. Earth Planet. Inter.*, 40, 77-134, 1985.
- Takeo, M., An inversion method to analyze the rupture processes of earthquakes using near-field seismograms, *Bull. Seismol. Soc. Am.*, 77, 490-513, 1987.
- Turcotte, D. L., A fractal model for crustal deformation, *Tectonophysics*, 192, 261-269, 1986.
- Utsu, T., Statistical study on the occurrence of aftershocks, *Geophys. Mag.*, 30, 521-605, 1961.
- Utsu, T., A method for determining the value of  $b$  in a formula  $\log n = a - bM$  showing the magnitude-frequency relation for earthquakes (in Japanese), *Geophys. Bull.* 13, pp. 99-103, Hokkaido Univ., Hokkaido, Japan, 1965.
- Utsu, T., Aftershocks and earthquake statistics I, Some parameters which characterize an aftershock sequence and their interaction, *J. Fac. Sci. Hokkaido Univ., Ser. 7*, 3, 129-195, 1969.
- Utsu, T., Aftershocks and earthquake statistics II, Further investigation of aftershocks and other earthquake sequences based on a new classification of earthquake sequences, *J. Fac. Sci., Hokkaido Univ., Ser. 7*, 3, 197-266, 1970.
- Utsu, T., Seismicity of the Izu peninsula and its vicinity from 1901 through 1980 with some remarks on the characteristics of foreshock activities, *Bull. Earthquake. Res. Inst. Univ. Tokyo*, 56, 25-41, 1981.
- Utsu, T., Y. Ogata, and R.S. Matsu'ura, The centenary of the Omori formula for a decay law of the aftershock activity, *J. Phys. Earth*, 43, 1-33, 1995.
- Yamanaka, Y., and K. Shimazaki, Scaling relationship between the number of aftershocks and the size of the main shock, *J. Phys. Earth*, 38, 305-324, 1990.
- Yamashita, T., and L. Knopoff, Models of aftershock occurrence, *Geophys. J. R. Astron. Soc.*, 91, 13-26, 1987.
- Yoshii, T., Proposal of the "aseismic front" (in Japanese), *J. Seismol. Soc. Jpn.*, 28, 365-367, 1975.

Z. Guo and Y. Ogata, Department of Statistical Science, The Graduate University for Advanced Studies, 4-6-7 Minami-azabu, Minato-ku, Tokyo 106, Japan. (e-mail: guo@ism.ac.jp, ogata@ism.ac.jp)

(Received February 1, 1996, revised September 20, 1996, accepted September 26, 1996.)